Department of Physics and Astronomy
Heidelberg University

Bachelor Thesis in Physics
submitted by

Luis Yagüe Bosch

born in Düsseldorf (Germany)

2023

Can adiabatic quantum gates be enhanced using counterdiabatic driving?

This Bachelor Thesis has been carried out by Luis Yagüe Bosch at the
Institute for Theoretical Physics in Heidelberg
under the supervision of
Prof. Sandro Wimberger
Prof. Luca Amendola

Abstract

Controlling quantum systems with the aim of utilizing their properties for new technology has been a broad subject of research in recent years and bears great potential for advancements in the near future. Implementing fast and high-fidelity quantum gates is essential for the realization of new quantum computers in the next years. This thesis explores how fast-oscillating Hamiltonians can be utilized to accelerate and improve entangling quantum gates. Our work is based on a protocol for an adiabatic CZ gate, in which symmetric laser pulses are applied on cold neutral Rydberg atoms. We apply a scheme that allows emulating counterdiabatic driving using real Hamiltonians and thus can correct diabatic errors as well as an unwanted phase. We analyze the error stability of the resulting gate and implement it into a simple quantum error correction circuit in the form of a CNOT gate.

Kurzfassung

Die Kontrolle quantenmechanischer Systeme mit dem Ziel ihre Möglichkeiten für neue Technologien zu nutzen ist wichtiger Gegenstand der Forschung der letzten Jahre und bietet großes Potential für zukünftige Entwicklungen. Die Realisierung eines schnellen Quantengatters mit hoher Fidelität ist Grundlage für den Bau von Quantencomputern in den nächsten Jahren. In dieser Arbeit befassen wir uns damit, wie schnell oszillierende Hamiltonians für die Beschleunigung und Verbesserung verschränkender Quantengatter genutzt werden können. Die Arbeit baut auf einem Protokoll für ein adiabatisches CZ-Gatter auf, in welchem symmetrische Laserpulse auf kalte, neutrale Rydberg-Atome angewendet werden. Wir wenden eine Methode an, die es erlaubt "counterdiabatic driving" mit reellen Hamiltonians zu emulieren und dadurch diabatische Fehler sowie einen zusätzliche Phase zu korrigieren. Wir testen das resultierende Gatter auf seine Stabilität und implementieren es in einem einfachen Quantenfehlerkorrektur-Schaltkreis in der Form eines CNOT-Gatters.

Contents

1 Introduction

Physics was revolutionized in the early 20th century with the formulation of quantum mechanics by physicists like Schrödinger, Heisenberg, and later von Neumann. Problems that could not be explained by classical physics could now be described using this newly developed formalism [1, pp. 3-4]. Ever since, quantum mechanics has become an indispensable theory to describe the world around us, spanning all fields of natural sciences [2, pp. 2-12].

However, it took another few decades until researchers started to go from merely describing the world around us using quantum mechanics, to controlling quantum mechanical systems and manipulating them for new purposes. In the late 60s and 70s researchers like Stratonovich, Helstrom and Gordon [3, 4] worked out a quantum mechanical formulation for optical communications, laying the foundations of a new field now called quantum information theory. Motivated by the success of classical information theory and computers in the 80s and 90s, David Deutsch and Richard Jozsa among others started developing algorithms based on quantum systems [5, 6]. Such algorithms promise to solve problems that cannot be efficiently solved on a classical computer, one of the most famous examples of this being Shor's algorithm for the factorization of prime numbers [7]. Around the same time, Richard Feynman pointed out that classical computers would have significant problems simulating quantum mechanical systems, which could be avoided by constructing a computer based on quantum systems [8]. This set the start for the modern evolution of quantum computers, which have grown into a promising platform for a broad band of applications.

There are various platforms for quantum computers being discussed in present research, examples being superconducting circuits, trapped ions and trapped neutral atoms [9, pp. 1-2]. In this thesis, we will discuss the latter in form of strongly interacting Rydberg atoms. The idea is to encode information in the internal states of the atoms and to make use of the atom-atom interaction of higher excited Rydberg states. Cold neutral atoms can be trapped in lattices using optical tweezers and excited using coherent lasers, such methods already allow arrays containing up to > 100 qubits [10].

In the first chapter, we will introduce a description of the Rydberg platform in more detail and show, how we can use laser pulses to construct simple gates, operating on two-qubit systems. We will further introduce the concept of counterdiabatic driving and effective counterdiabatic driving, which is a powerful method to increase gate fidelities and accelerate gate times. In the second chapter, we will discuss the applicability of these methods to an adiabatic controlled-phase (or CZ) gate in order to improve the gate regarding fidelity and protocol time. We will then test the gate for its stability under experimental errors. In order to test the CZ gate in the context of a simple quantum algorithm, we will extend it to a CNOT gate and implement it into a simple quantum error correction circuit. In the last section, we will address the problem of having to drive two-qubit terms in order to realize the Hamiltonian and discuss an approach for a possible workaround.

2 Physics background

To understand the results presented throughout this thesis, we have to introduce a variety of physical concepts, which is the purpose of the following chapter. We start by introducing the interaction between a qubit system with a laser which we then extend to the Rydberg platform and how it interacts with lasers. We continue by discussing a set of two-qubit quantum gates that can be implemented on the Rydberg platform. The chapter is concluded by introducing the concepts of counterdiabatic driving and effective counterdiabatic driving, which can be used to enhance the performance of quantum gates.

2.1 Qubit systems and adiabatic driving

Landau-Zener Hamiltonian and ARP-pulses

Before concerning ourselves with the three-state quantum systems we will end up using throughout the thesis, it is worth having a look at more simple two-state systems. Some problems in the three or more state systems can be reduced to the problems we discuss in the following. Furthermore, it will hold as an exemplary system to introduce new concepts later on in the chapter.

The Landau-Zener system describes the application of a pulse with frequency ω_L on a system of two states $|0\rangle$ and $|1\rangle$. Lev Landau and Clarence Zener discussed the system first in 1932 among others [11, 12, 13, 14]. The derivation presented here follows an approach similar to [15, pp. 5-6] and [16, pp. 13-15]. The Hamiltonian of the system can be written as

$$H(t) = E_0|0\rangle\langle 0| + E_1|1\rangle\langle 1| + \hat{\boldsymbol{d}}\boldsymbol{E} \tag{2.1}$$

where $\hat{\boldsymbol{d}}$ is the dipole operator and $\boldsymbol{E} = \boldsymbol{E}_L \cos(\omega_L t)$ the electric field. We define the Rabi frequency

$$\Omega = \frac{\langle 0|\hat{\boldsymbol{d}}\boldsymbol{E}|1\rangle}{\hbar} \tag{2.2}$$

as well as $\omega_{01} = (E_1 - E_0)/\hbar$. The diagonal entries of the dipole moment are zero, meaning we can write $\hat{\boldsymbol{d}}\boldsymbol{E} = \hbar\Omega\cos(\omega_L t)(|0\rangle\langle 1| + |1\rangle\langle 0|)$. Thus, the Hamiltonian can be rewritten in matrix form

$$H(t) = \hbar \begin{pmatrix} 0 & \Omega\cos(\omega_L t) \\ \Omega\cos(\omega_L t) & \omega_{01} \end{pmatrix} \tag{2.3}$$

after shifting it by a for the dynamics irrelevant amount of $\mathbb{1}E_0$. Next, we go into a rotating frame by applying the unitary transformation

$$U = \begin{pmatrix} 1 & 0 \\ 0 & e^{i\omega_L t} \end{pmatrix}. \tag{2.4}$$

In order to keep the dynamics of the system, the Hamiltonian transforms as $H \to UHU^\dagger + i\hbar\dot{U}U^\dagger$. A calculation reveals that in the rotating frame, the Hamiltonian reads

$$H(t) = \hbar \begin{pmatrix} 0 & \frac{\Omega}{2}\left(1 + e^{-2i\omega_L t}\right) \\ \frac{\Omega}{2}\left(1 + e^{2i\omega_L t}\right) & \omega_{01} - \omega_L \end{pmatrix} \tag{2.5}$$

The rotating wave approximation (RWA) states that we can neglect the fast oscillating terms if $|\omega_{01} - \omega_L|,\ |\Omega| \ll \omega_L$. After defining the detuning $\Delta = \omega_{01} - \omega_L$, the Hamiltonian reduces to

$$H(t) = \frac{\hbar}{2} \begin{pmatrix} 0 & \Omega \\ \Omega & 2\Delta \end{pmatrix}. \tag{2.6}$$

This is the standard form of the Landau-Zener Hamiltonian shifted by $\mathbb{1}\Delta$. The off-diagonal elements drive transitions between the ground state $|0\rangle$ and the excited state $|1\rangle$. A complete population transfer, i.e. a rotation of the state in the Bloch-sphere by π, can be achieved by applying a pulse of area $\int \mathrm{d}t\ \Omega(t) = \pi$ with zero detuning $\Delta(t) = 0$. Since such π-pulses depend on the exact area of the pulse, they are sensitive to pulse area errors. A more robust solution will be discussed in the next section.

Adiabatic theorem and ARP pulses

The adiabatic theorem in its original form was formulated by Max Born and Vladimir Fock [17]. It states that if a system is initially in an eigenstate, it remains an eigenstate, given that the Hamiltonian changes slowly enough and that there is a gap between the eigenvalue and the rest of the Hamiltonians spectrum. A process that fulfills these conditions is called adiabatic, a process that doesn't is called non-adiabatic or diabatic.
Choosing the Rabi frequencies and the detuning such that the adiabatic condition is fulfilled allows the evolution of an instantaneous eigenstate into the desired final state. For the Landau-Zener system, a complete adiabatic population transfer can be achieved by choosing a large Rabi frequency and a linear detuning $\Delta \propto t$, sweeping through the frequencies [18]. The Rabi pulse is usually chosen to be Gaussian, providing a continuous change of the Hamiltonian. These so-called adiabatic rapid passage (ARP) pulses are less dependent on the specific pulse area and more robust than π-pulses at the cost of requiring a slowly changing Hamiltonian. ARP pulses can be used for example to avoid populations of unstable intermediate states [19]. In the following, we will use ARP pulses as well as π-pulses in multi-qubit systems to create entangling quantum gates.

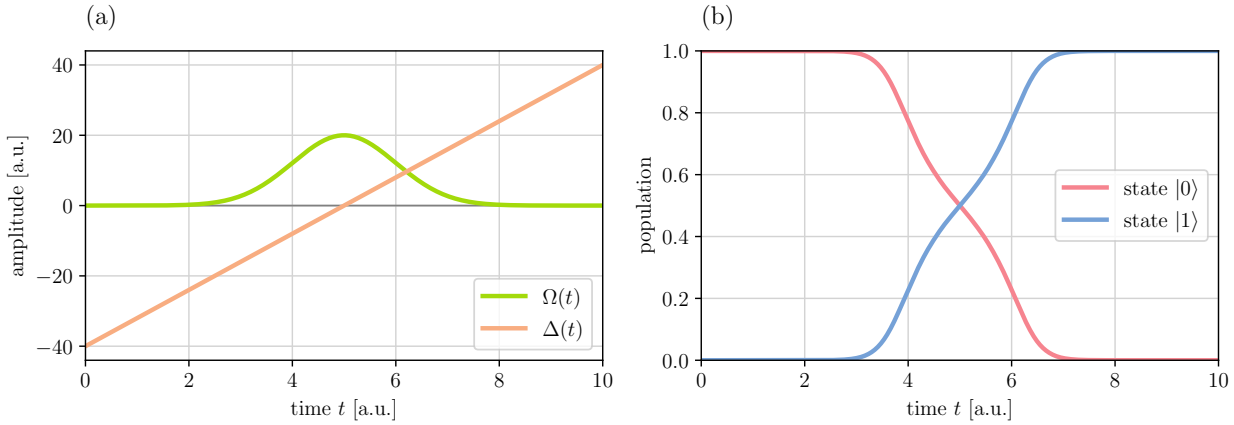

Figure 2.1: (a) ARP pulse with Gaussian-shaped Rabi pulse and linear detuning. (b) Population transfer of the Landau-Zener system under the ARP pulse from (a).

Fidelity

The fidelity is an important measure to quantify how well a quantum mechanical process (for example the application of a laser pulse on a qubit) performs. The fidelity between two density

matrices is most generally defined as [20]

$$\mathcal{F}(\rho,\sigma) := \left(\mathrm{tr}\sqrt{\sqrt{\rho}\sigma\sqrt{\rho}}\right)^2. \tag{2.7}$$

Depending on the textbook one might also find the same definition without a square [2, pp. 409-411]. The fidelity is symmetric in its inputs i.e. $\mathcal{F}(\rho,\sigma) = \mathcal{F}(\sigma,\rho)$. One can check that if one of the states is pure $\rho = |\psi_\rho\rangle\langle\psi_\rho|$, the fidelity can be written as

$$\mathcal{F}(|\psi_\rho\rangle,\sigma) = \langle\psi_\rho|\sigma|\psi_\rho\rangle. \tag{2.8}$$

If both states are pure, the fidelity reduces to the squared overlap between the states

$$\mathcal{F}(|\psi_\rho\rangle,|\psi_\sigma\rangle) = |\langle\psi_\rho|\psi_\sigma\rangle|^2. \tag{2.9}$$

We will use the fidelity mainly as a measure to calculate the overlap between a dynamically produced output state (e.g. after applying an ARP pulse) and the state we want to produce ideally.

2.2 Rydberg systems

For quantum computation, we need feasible quantum systems from which more complex quantum circuits can be constructed. One promising platform was first brought up by Jaksch et al. [21] in the form of cold neutral atoms with Rydberg states, also called Rydberg atoms or Rydberg qubits. They have since been used in a variety of ways to create entangling multi-qubit gates of which we will discuss a few in section 2.3. The Rydberg atoms we will use have two ground states $|0\rangle$ and $|1\rangle$ that are encoded in the hyperfine splitting and the highly excited Rydberg state $|r\rangle$. A key feature of Rydberg atoms is a strong long-range dipole-dipole interaction between two atoms that are in the excited Rydberg state. Typically, such systems are based on Alkali atoms like Li, K, Rb and Cs that are laser-cooled and trapped in optical traps [9, pp. 3-5].

Suppose we have a Rydberg atom on which we apply two lasers with frequencies ω_{L1} and ω_{L2} that drive the transitions $|0\rangle \leftrightarrow |1\rangle$ and $|1\rangle \leftrightarrow |r\rangle$. In a similar fashion to the derivation of the Landau-Zener Hamiltonian (2.6) one can show [15, pp. 5-6] [16, pp. 13-15] that in a rotating

frame the system is described by the Hamiltonian

$$H(t) = \frac{\hbar}{2} \begin{pmatrix} 0 & \Omega_{01} & 0 \\ \Omega_{01} & 2\delta & \Omega_{1r} \\ 0 & \Omega_{1r} & 2\Delta \end{pmatrix}. \tag{2.10}$$

where we defined

$$\delta := \omega_{01} - \omega_{L1}, \qquad \Delta := \omega_{01} + \omega_{1r} - \omega_{L1} - \omega_{L2}. \tag{2.11}$$

In the following, we will set $\hbar = 1$ and $\delta = 0$ as is commonly done. When describing a system of two or more Rydberg qubits, an additional coupling term with a coupling strength V appears to include the dipole-dipole interaction between two atoms in the Rydberg state. The Hamiltonian for a two Rydberg atom system thus reads

$$H_0(t) = H^{(A)}(t) \otimes \mathbb{1} + \mathbb{1} \otimes H^{(B)}(t) + V|r\rangle\langle r| \otimes |r\rangle\langle r|. \tag{2.12}$$

In this thesis, we mainly look at systems that are made up of two Rydberg atoms so in most cases we refer to this Hamiltonian. Large Rydberg interactions $V \gg \Omega, \Delta$ cause high energy levels of the Rydberg interacting two-qubit state $|rr\rangle$. This causes a blockade of said state: the presence of a Rydberg excited atom $|r\rangle$ shifts the energy level of a second nearby atom so that it will hardly be excited by the laser [22, p. 1]. We will exploit this so-called Rydberg blockade mechanism for constructing two-qubit entangling gates. The Rydberg interaction scales with n^{11} where n is the principal quantum number, such that values for V up to a few GHz can be found in the literature [23, 24] and has been demonstrated for neutral atoms with separation $> 10\ \mu$m [25].

2.3 Quantum gates

Classical computer circuits are based on transforming binary inputs using different types of Boolean logic gates [26, pp. 51-60]. In this thesis, we will put a large focus on the controlled-NOT (or CNOT) gate, which is a two-bit gate, crucial for quantum computing. The CNOT gate changes the second bit if and only if the first bit is 1. It is reversible, which means that it does not erase any information or in other words, every output corresponds to a unique input. Similar to the classical case, any operation on a qubit can be decomposed into a series of quantum logic gates acting on it [26, pp. 69-87]. The similarities between classical and quantum

computers were discussed early on for example by Richard Feynman [27] and David Deutsch [28]. In contrast to its classical counterpart, a qubit can assume an infinite amount of superpositions of 0 and 1, thus providing new possibilities that can be made use of in new quantum computers. It follows from the Schrödinger equation that the time evolution of a quantum mechanical state in an isolated system can be described by a unitary operator $U(t)$ such that $|\psi(t)\rangle = U(t)|\psi(0)\rangle$. Therefore a quantum logic gate can always be represented by a unitary matrix evolving the initial state $|\psi(0)\rangle$ into a final state $|\psi(t)\rangle$. Because the evolution matrix is unitary, quantum gates are always logically reversible. Furthermore, any two-qubit operation can be carried out by using only CNOT and single-qubit gates [2, p. 191]. Therefore it is of great interest to develop a high-fidelity, fast and stable CNOT quantum gate.
We already discussed Rydberg atoms as a platform for quantum computing in the previous section. Implementations of adiabatic and non-adiabatic entangling quantum gates based on Rydberg atoms and Rydberg interactions have been demonstrated theoretically and experimentally [21, 24, 23, 29, 30, 31]. Such gates have shown to be robust against errors like those caused by thermal motion of atoms [29]. In the following we will introduce various two-qubit gates based on Rydberg atoms, culminating in the implementation of a CZ-based CNOT gate.

Rydberg CPHASE gate

A first example of an entangling gate that exploits the Rydberg interaction is the CPHASE gate as it was first introduced by Jaksch et al. [21]. In the computational basis $\{|00\rangle, |01\rangle, |10\rangle, |11\rangle\}$ the CPHASE gate reads

$$\text{CPHASE} = \begin{bmatrix} e^{i\phi_{00}} & 0 & 0 & 0 \\ 0 & e^{i\phi_{01}} & 0 & 0 \\ 0 & 0 & e^{i\phi_{10}} & 0 \\ 0 & 0 & 0 & e^{i\phi_{11}} \end{bmatrix}. \tag{2.13}$$

Let us assume for now a mid-range Rydberg interaction i.e. $V \sim \Omega, \Delta$. The gate can be realized, by applying two π pulses on both atoms, driving the transition $|1\rangle \leftrightarrow |r\rangle$, with a waiting period τ in between. During the waiting period, the state $|rr\rangle$ gains a phase of $-V\tau$ under the presence of the Rydberg interaction. Furthermore all states except $|00\rangle$ gain a dynamical phase $-\pi/2$ during the application of the pulses, causing the protocol to act onto the computational basis

states as

$$\begin{aligned}
|00\rangle &\xrightarrow{\Omega_{1r}} |00\rangle \xrightarrow{\tau} |00\rangle \xrightarrow{\Omega_{1r}} |00\rangle,\\
|01\rangle &\xrightarrow{\Omega_{1r}} -i|0r\rangle \xrightarrow{\tau} -i|0r\rangle \xrightarrow{\Omega_{1r}} -|01\rangle,\\
|10\rangle &\xrightarrow{\Omega_{1r}} -i|r0\rangle \xrightarrow{\tau} -i|r0\rangle \xrightarrow{\Omega_{1r}} -|10\rangle,\\
|11\rangle &\xrightarrow{\Omega_{1r}} -|rr\rangle \xrightarrow{\tau} -e^{-iV\tau}|r1\rangle \xrightarrow{\Omega_{1r}} e^{-iV\tau}|11\rangle.
\end{aligned}$$

This protocol produces a CPHASE gate with $\phi_{00} = 0$, $\phi_{01} = \phi_{10} = \pi$ and $\phi_{11} = -V\tau$. The gate is not very robust, as it is sensitive to the interaction strength, an issue that we will tackle in the next subsection.

Non-adiabatic CZ gate

The sensitivity of the CPHASE gate motivates us to make use of the Rydberg blockade mechanism i.e. to work with $V \gg \Omega, \Delta$. This way, the fidelity of the gate will rather depend on how well the blockade is working instead of the exact value of V. A special instance of a CPHASE gate is the controlled-Z (or CZ) gate, fixing $\phi_{00} = 0$ and $\phi_{01} = \phi_{10} = \phi_{11} = \pi$. In the computational basis, it reads

$$\mathrm{CZ} = \begin{bmatrix} 1 & 0 & 0 & 0 \\ 0 & -1 & 0 & 0 \\ 0 & 0 & -1 & 0 \\ 0 & 0 & 0 & -1 \end{bmatrix}. \tag{2.14}$$

Depending on the literature one might also find the relative minus between $|11\rangle$ and the other states. An approach to realize a CZ gate in the high Rydberg interaction regime was also proposed by Jaksch et al. in the same paper as the CPHASE gate [21]. The protocol consists of a π pulse driving the transition $|1\rangle \leftrightarrow |r\rangle$ on the first qubit, a 2π pulse driving the same transition on the second qubit and finally a repeated application of the first pulse. During the second pulse, the Rydberg blockade prohibits state $|r1\rangle$ from being excited into $|rr\rangle$. Taking also into account the dynamical phases of $\pi/2$ and π caused by the pulses, the protocol evolves

the states as follows:

$$
\begin{aligned}
|00\rangle &\xrightarrow{\Omega_{1r}^{(\mathrm{A})}} |00\rangle \xrightarrow{\Omega_{1r}^{(\mathrm{B})}} |00\rangle \xrightarrow{\Omega_{1r}^{(\mathrm{A})}} |00\rangle, \\
|01\rangle &\xrightarrow{\Omega_{1r}^{(\mathrm{A})}} |01\rangle \xrightarrow{\Omega_{1r}^{(\mathrm{B})}} -|01\rangle \xrightarrow{\Omega_{1r}^{(\mathrm{A})}} -|01\rangle, \\
|10\rangle &\xrightarrow{\Omega_{1r}^{(\mathrm{A})}} -i|r0\rangle \xrightarrow{\Omega_{1r}^{(\mathrm{B})}} -i|r0\rangle \xrightarrow{\Omega_{1r}^{(\mathrm{A})}} -|10\rangle, \\
|11\rangle &\xrightarrow{\Omega_{1r}^{(\mathrm{A})}} -i|r1\rangle \xrightarrow{\Omega_{1r}^{(\mathrm{B})}} -i|r1\rangle \xrightarrow{\Omega_{1r}^{(\mathrm{A})}} -|11\rangle.
\end{aligned}
$$

As said before, this gate tends to be more robust than the CPHASE gate as it does not depend on the exact value of V. For finite Rydberg blockades, a small population will be excited to $|rr\rangle$ and cause a population error for the $|11\rangle$ state. It is also known that a small phase error is introduced in state $|11\rangle$ due to an imperfect Rydberg blockade. This is discussed in more detail in the thesis of Tim Ehret [15, pp. 14-15].

Adiabatic CZ gate

Saffman et al. [23] proposed an adiabatic implementation of a CZ gate. Tim Ehret modified said protocol by including a continuous detuning [15, pp. 18-19]. The protocol consists of two Gaussian-like pulses applied at the same time on both Rydberg atoms. Only the transition $|1\rangle \leftrightarrow |r\rangle$ is driven on both atoms simultaneously i.e. $\Omega_{1r}^{(A)}(t) = \Omega_{1r}^{(B)}(t) \equiv \Omega(t)$ and $\Omega_{01}^{(A)}(t) = \Omega_{01}^{(B)}(t) = 0$. The detuning consists of two sine waves applied at the same time as the Gaussian pulses and a third sine wave in between to avoid a discontinuous jump.

$$
\Omega(t) = \begin{cases}
\frac{\Omega_{\max}}{1-a_1}\left(\exp\left(-\frac{(t-T/4)^4}{\tau^4}\right) - a_1\right) & 0 \le t \le T/2 \\
0 & T/2 \le t \le T/2 + T_2 \\
\frac{\Omega_{\max}}{1-a_2}\left(\exp\left(-\frac{(t-T_2-3T/4)^4}{\tau^4}\right) - a_2\right) & T/2 + T_2 \le t \le T + T_2,
\end{cases} \tag{2.15}
$$

$$
\Delta(t) = \begin{cases}
\Delta_{\max}\cos\left(\frac{2\pi t}{T}\right) & 0 \le t \le T/2 \\
-\Delta_{\max}\cos\left(\frac{\pi(t-T/2)}{T_2}\right) & T/2 \le t \le T/2 + T_2 \\
\Delta_{\max}\cos\left(\frac{2\pi(t-T_2)}{T}\right) & T/2 + T_2 \le t \le T + T_2
\end{cases} \tag{2.16}
$$

The offsets a_1 and a_2 are chosen such that the amplitude vanishes at the start and stop points i.e. $\Omega(0) = \Omega(T) = 0$. The parameters $\Omega_{\max}$ and $\Delta_{\max}$ determine the maximum height of the respective function, τ is the width of the Gaussian and T_2 corresponds to the pause between both pulses. The total protocol time is $T_{\mathrm{tot}} = T + T_2$.

The protocol generates a phase of π for the initial states $|01\rangle$, $|10\rangle$ and $|11\rangle$. State $|00\rangle$ is not affected by the pulses at all so it remains in its initial state. The time evolution of state $|11\rangle$ can be seen in Fig. 2.2b and c.

A known issue of the gate is the collection of an unwanted dynamical phase by the state $|11\rangle$ similar to the non-adiabatic CZ gate, such that it evolves as $|11\rangle \to -e^{\phi_r}|11\rangle$. The phase is not a product of diabatic evolution but of an imperfect Rydberg blockade. A detailed discussion can be found in [15, pp. 23-25], where it is also shown that the phase can be approximated by

$$\phi_r \approx -\int_0^{T_{\text{tot}}} \mathrm{d}t\, \frac{\Omega^2}{4V} \propto \frac{T_{\text{tot}}\Omega_{\text{max}}^2}{V}. \tag{2.17}$$

Although the Rydberg blockade can be chosen quite large, a finite blockade still causes small errors. The presented phase error is an issue for superpositions of $|11\rangle$ with other states. Next to the presented phase issue, an imperfect Rydberg blockade also causes small diabatic errors. Both these problems will be the subject of discussions in this thesis.

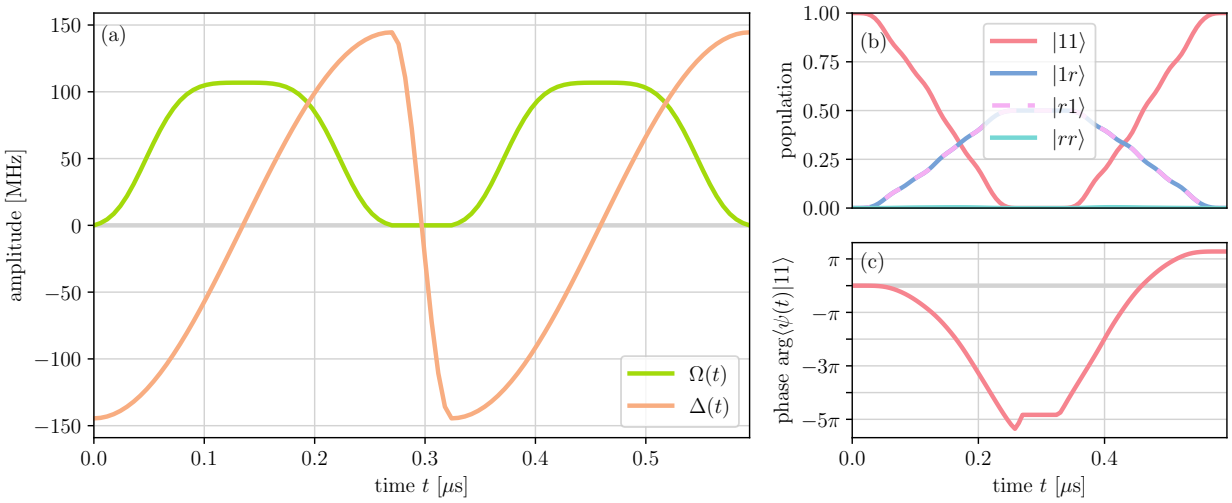

Figure 2.2: (a) Rabi frequency $\Omega(t)$ and detuning $\Delta(t)$ for the implementation of the adiabatic CZ gate including a continuous detuning. (b) Exemplary time evolution of the populations with initial state $|11\rangle$ under the adiabatic CZ gate and (c) the phase accumulated in state $|11\rangle$. Notice that the generated phase in the end is different from π due to the unwanted dynamical phase. The plateau in the phase is due to the pulses being switched off. The parameters for the pulses are the same as in the Saffman paper $\Omega_{\text{max}}/2\pi = 17$ MHz, $\Delta_{\text{max}}/2\pi = 23$ MHz, $T = 0.54$ μs, $T_2 = T/10$, $\tau = 0.175T$.

CNOT gate

In the computational basis of a two qubit system $\{|00\rangle, |01\rangle, |10\rangle, |11\rangle\}$ the CNOT gate reads

$$\text{CNOT} = \begin{bmatrix} 1 & 0 & 0 & 0 \\ 0 & 1 & 0 & 0 \\ 0 & 0 & 0 & 1 \\ 0 & 0 & 1 & 0 \end{bmatrix}. \tag{2.18}$$

The CNOT gate can be constructed using the previously introduced CZ gate and single-qubit rotations. The sequence we will use to construct to extend our CNOT gate is the following:

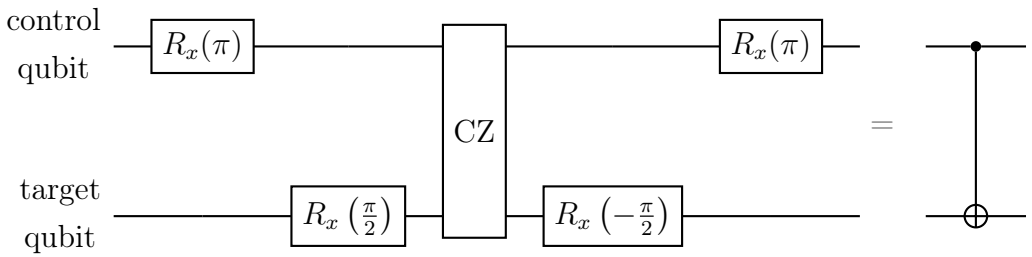

where the gate on the right-hand side shows a CNOT gate. It was presented by Tim Ehret [15, pp. 9-11] and uses the single qubit rotation matrices

$$R_x(\theta) = \begin{bmatrix} \cos\left(\frac{\theta}{2}\right) & -i\sin\left(\frac{\theta}{2}\right) \\ -i\sin\left(\frac{\theta}{2}\right) & \cos\left(\frac{\theta}{2}\right) \end{bmatrix}, \tag{2.19}$$

$$R_y(\theta) = \begin{bmatrix} \cos\left(\frac{\theta}{2}\right) & -\sin\left(\frac{\theta}{2}\right) \\ \sin\left(\frac{\theta}{2}\right) & \cos\left(\frac{\theta}{2}\right) \end{bmatrix}. \tag{2.20}$$

In this thesis, we will focus on the CZ gate, which we can later turn into a CNOT gate assuming we have perfect single-qubit operations. Even if we discuss the CZ gate most of the time, one should keep in mind that this is done with the intent of constructing a CNOT gate.

2.4 Counterdiabatic driving

When a state is prepared in an eigenstate of the Hamiltonian $H_0(0)$ and the Hamiltonian varies sufficiently slow in time, according to the adiabatic theorem the state follows the instantaneous eigenstate of the Hamiltonian $H_0(t)$. As long as the Hamiltonian acts on a finite time scale, transition amplitudes between instantaneous eigenstates are not exactly zero and if one tries to implement faster gates these diabatic errors become larger. During the past years, a lot of

efforts have been made to achieve adiabatic evolution even on short time scales [32]. A particular approach was first utilized by Demirplak and Rice [33] and later by Berry [34], although similar ideas have been brought up before [35]. We follow here the approach of Berry, also presented in [15, p. 8]. Consider a Hamiltonian with nondegenerate eigenstates $|n(t)\rangle$ and eigenenergies $E_n(t)$

$$H_0(t)|n(t)\rangle = E_n(t)|n(t)\rangle. \tag{2.21}$$

For the adiabatic approximation, states prepared in the eigenstate $|\psi_n(0)\rangle = |n(0)\rangle$ remain in the instantaneous eigenstate, only gaining a phase $\gamma(t)$, given by

$$\gamma(t) = -\frac{1}{\hbar}\int_0^t \mathrm{d}t'\ E_n(t') + \int_0^t \mathrm{d}t'\ \langle n(t')|\partial_{t'} n(t')\rangle, \qquad |\psi_n(t)\rangle = e^{i\gamma_n(t)}|n(t)\rangle. \tag{2.22}$$

If the adiabatic states are the exact solutions of the Schrödinger equation, transitions can be completely avoided. We therefore search for a Hamiltonian that satisfies $i\hbar\partial_t|\psi_n(t)\rangle = H(t)|\psi_n(t)\rangle$. A unitary time evolution $U(t)$ solves the Schrödinger equation $i\hbar\partial_t U(t) = H(t)U(t)$ if

$$H(t) = i\hbar(\partial_t U(t))U^\dagger(t). \tag{2.23}$$

Furthermore one can fulfill $U(t)|n(0)\rangle = |\psi_n(t)\rangle$ by choosing

$$U(t) = \sum_n e^{i\gamma_n(t)}|n(t)\rangle\langle n(0)|. \tag{2.24}$$

Inserting (2.24) into (2.23) yields

$$H(t) = \underbrace{\sum_n |n(t)\rangle E_n(t)\langle n(t)|}_{=H_0(t)} + \underbrace{i\hbar\sum_n \left(|\partial_t n(t)\rangle\langle n(t)| - \langle n(t)|\partial_t n(t)\rangle|n(t)\rangle\langle n(t)|\right)}_{=:H_{\mathrm{CD}}(t)}. \tag{2.25}$$

The additional term $H_{\mathrm{CD}}(t)$ we encounter in this new total Hamiltonian is called the counter-diabatic (CD) Hamiltonian. By noticing that after differentiating (2.21) we get

$$\langle m|\partial_t n\rangle = \frac{\langle m|\partial_t H_0|n\rangle}{E_n - E_m} \tag{2.26}$$

the explicit derivative $|\partial_t n\rangle$ can be eliminated and H_{CD} can be rewritten to

$$H_{\mathrm{CD}} = \sum_{n\neq m} \frac{|n\rangle\langle n|\partial_t H_0|m\rangle\langle m|}{E_m - E_n}. \tag{2.27}$$

Adding this counterdiabatic Hamiltonian to the original Hamiltonian completely prevents diabatic evolution i.e. transitions between instantaneous eigenstates in the system.
Another perspective is presented in [36, p. 2]. Under an arbitrary unitary transformation, the Hamiltonian transforms as $H_0 \to U^\dagger H_0 U - iU^\dagger \dot{U}$. With the right choice of U, we can diagonalize the first term while the second term produces off-diagonal elements. However, this second term can be canceled by adding an extra

$$H_{\mathrm{CD}} = i\dot{U}U^\dagger \tag{2.28}$$

to H_0. Then the instantaneous eigenstates of $H_0 + H_{\mathrm{CD}}$ remain eigenstates of H_0 and evolve into the desired final states. Thus, we can also calculate H_{CD} by finding a U that diagonalizes H_0, which can be done well for few-level systems by finding its eigenvectors.

Example: Landau-Zener CD-driving

Given a Landau-Zener Hamiltonian as in (2.6) one can show that the instantaneous eigenvectors of H_0 are

$$v = \left\{ \begin{pmatrix} -\sin\theta \\ \cos\theta \end{pmatrix}, \begin{pmatrix} \cos\theta \\ \sin\theta \end{pmatrix} \right\}, \tag{2.29}$$

where $\theta = \frac{1}{2}\arctan(-\Omega/\Delta)$ [36, pp. 2-3]. The Hamiltonian can thus be diagonalized by the unitary matrix

$$U = \begin{pmatrix} -\sin\theta & \cos\theta \\ \cos\theta & \sin\theta \end{pmatrix}. \tag{2.30}$$

The CD Hamiltonian follows directly from that by using (2.28)

$$H_{\mathrm{CD}} = \begin{pmatrix} 0 & -i\dot{\theta} \\ i\dot{\theta} & 0 \end{pmatrix}. \tag{2.31}$$

The full Hamiltonian $H = H_0 + H_{\mathrm{CD}}$ will prevent diabatic evolution of the system. If we take $\Omega(0) = \Omega(T) = 0$, the initial and final eigenstates turn out to be $|0\rangle$ and $|1\rangle$. Under adiabatic evolution, a qubit prepared in one of the eigenstates will evolve into either eigenstate, gaining a phase at most.

2.5 Effective counterdiabatic driving

For any non-degenerate system described by a time-dependent Hamiltonian, we can calculate a counterdiabatic Hamiltonian using (2.27). However, when facing quantum systems in practice,

one only has access to limited realizable Hamiltonians. The desirable Hamiltonian may not necessarily be constructed from the available setup, which can only control certain interactions on the system. A workaround for this problem was proposed by Petiziol et al. [37], using the initially available interactions controlled by $H_0(t)$ to construct an effective counterdiabatic field $H_{\mathrm{E}}(t)$ that emulates $H_{\mathrm{CD}}(t)$.

The time evolution of a state from a given initial time t_n to $t_n + T$ is unitary under the Schrödinger equation and can be described by a unitary time evolution operator $U(T)$ or in exponential form $\exp(M(T))$. The exponent $M(T)$ can be written as an infinite sum in a so-called Magnus expansion $M(T) = \sum_i M^{(i)}(T)$. The first two terms of this expansion read

$$M^{(1)}(T) = -\frac{i}{\hbar}\int_{t_n}^{t_n+T} \mathrm{d}t'\ H(t') \tag{2.32}$$

$$M^{(2)}(T) = -\frac{1}{2}\left(\frac{i}{\hbar}\right)^2 \int_{t_n}^{t_n+T} \mathrm{d}t' \int_{t_n}^{t_n+t'} \mathrm{d}t''\ [H(t'), H(t'')]. \tag{2.33}$$

Higher order terms can also be calculated but are not necessary for our purpose. We divide the time in a finite grid t_n with size $t_{n+1} - t_n = T =: 2\pi/\omega$. The idea is to approximate the time evolution caused by H_{CD} between two times by using only the first term of its Magnus expansion (i.e. approximating in the first order of $1/\omega$) and then finding a suitable "effective counterdiabatic" (E-CD) Hamiltonian H_{E} that emulates this approximated time evolution using the available controls. We usually take ω to be large compared to the other quantities in the system in order for the approximation to work. We choose H_{E} (i) such that the first order term $M_{\mathrm{E}}^{(1)}$ vanishes and (ii) to be proportional to $\sqrt{\omega}$ so we can emulate $M_{\mathrm{CD}}^{(1)}$ using the second-order Magnus expansion of the effective field

$$M_{\mathrm{CD}}^{(1)}(T) = M_{\mathrm{E}}^{(2)}(T). \tag{2.34}$$

We need condition (i) so that the leading contribution is the second Magnus term, containing the commutator of $H_{\mathrm{E}}(t)$ with itself, which allows us to drive matrix elements not directly targeted by H_{E}. Condition (ii) is important so that $M_{\mathrm{E}}^{(2)}$ is of the same order in ω as $M_{\mathrm{CD}}^{(1)}$. These conditions are met by making the ansatz

$$H_{\mathrm{E}}(t) = \sqrt{\omega}\sum_i c_i(t) H_i, \tag{2.35}$$

$$c_i(t) = \sum_{k=1}^{L} \left[A_{ik}(t)\sin(k\omega t) + B_{ik}(t)\cos(k\omega t)\right], \tag{2.36}$$

where H_i are time-independent matrices. Usually, H_i are obtained as a decomposition of the original Hamiltonian into control functions $H_0(t) = \sum_i u_i(t)H_i$. One can show that it is always possible to successfully construct H_E from a suitable choice of control functions [37, pp. 2-4]. Note that we could also include terms of higher order in $1/\omega$ i.e. higher terms in the Magnus expansion to improve results. However, one can make the error arbitrarily small by choosing ω large enough and a first-order Magnus approximation suffices in our case.

Example: Landau-Zener E-CD driving

As seen in (2.31), the counterdiabatic Hamiltonian for the Landau-Zener problem contains imaginary elements on the off-diagonals such that an experimental implementation is difficult. We can overcome this issue by constructing an effective CD Hamiltonian. In this case, the system allows us to make the ansatz

$$H_\mathrm{E}(t) = \sqrt{\omega}\begin{pmatrix} c_1(t) & c_2(t) \\ c_2(t) & -c_1(t) \end{pmatrix} = c_1(t)\sigma_z + c_2(t)\sigma_x. \tag{2.37}$$

A calculation reveals (see A.3) that the second-order Magnus term is given by

$$\begin{aligned} M_\mathrm{E}^{(2)}(T) &= iT\sum_{k=1}^{L}\left(A_{1k}B_{2k} - B_{1k}A_{2k}\right)\sigma_y \\ &= iT\left(A_{11}B_{21} - B_{11}A_{21}\right)\sigma_y \end{aligned} \tag{2.38}$$

where in the second line we set $L = 1$ and the coefficients A_{ik} and B_{ik} are evaluated at t_n. The first-order Magnus term of the CD Hamiltonian is given by

$$M_\mathrm{CD}^{(1)}(T) = -i\int_{t_n}^{t_n+T}\mathrm{d}t'\ \dot{\theta}(t')\sigma_y \approx -iT\dot{\theta}(t_n)\sigma_y. \tag{2.39}$$

To obtain the desired time evolution, the condition $M_\mathrm{CD}^{(1)}(T) = M_\mathrm{E}^{(2)}(T)$ must be fulfilled. This can for example be done by choosing $A_{11} = B_{21} = 0$ and

$$A_{21} = \sqrt{|\dot{\theta}|} \equiv A, \qquad B_{11} = \mathrm{sgn}(\dot{\theta})\sqrt{|\dot{\theta}|} \equiv B. \tag{2.40}$$

The E-CD Hamiltonian takes the form

$$H_{\mathrm{E}}(t) = \sqrt{\omega} \begin{pmatrix} B\cos(\omega t) & A\sin(\omega t) \\ A\sin(\omega t) & -B\cos(\omega t) \end{pmatrix}. \tag{2.41}$$

The results of using this effective counterdiabatic driving compared to 'true' CD driving can be seen in fig. 2.3. Fidelity improvements by effective CD driving have already been discussed in more detail for more complicated systems [38]. It was previously mentioned that the error becomes smaller in the limit of high ω, because higher order Magnus terms contribute with higher orders of $1/\omega$. A quantitative analysis of this for the Landau-Zener system can be found in A.1.

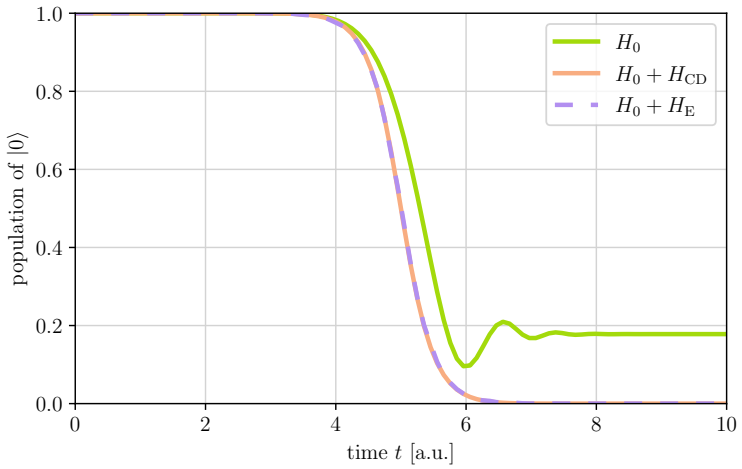

Figure 2.3: Population transfer of the ground state $|0\rangle$ for different driving methods: using only a (non-adiabatic) Gaussian pulse (green), using CD driving (orange) and using effective counterdiabatic driving (purple).

2.6 Numerics

We use the python modules QuTip [39] and NumPy [40] for most of our simulations. Given a Hamiltonian, the time evolution of arbitrary state vectors and density matrices can be obtained using QuTip's `sesolve` function, which is a solver for the Schrödinger equation. We can test the solver by calculating the time evolution of the input state $|0\rangle$ under a π pulse and determining the infidelity. The numerical errors produced this way were of order $< 10^{-11}$. This is accurate enough for our purposes; infidelities due to diabatic evolution in the cases discussed in this thesis are usually of order $> 10^{-5}$. It is also worth noticing that the results were relatively inde-

pendent of the number of iterations used. For the E-CD driving we sometimes had to increase the number of iterations because the Hamiltonian is rapidly changing, but in most cases, a few hundred to thousand timesteps sufficed to obtain converging results.
Another crucial part is the development of a good algorithm to calculate counterdiabatic Hamiltonians. While it might be possible to calculate them analytically for simple systems, it can get tedious quite fast for larger ones. An implementation in python included using (2.27) and numerical estimation of the eigenvectors and eigenvalues using NumPy's `linalg.eigh` function. It suffices to calculate H_{CD} for a few hundred times and use QuTip's `Cubic_Spline` function to quadratically interpolate between these points. We were able to test our numerical CD Hamiltonian by comparing it to known analytical results e.g. for the Landau-Zener system or the adiabatic CZ gate as derived in section 3.1. The absolute errors were of order $< 10^{-11}$ which is well in the region of numerical noise.

3 E-CD driving of the adiabatic CZ gate

Counterdiabatic driving is a useful tool to accelerate a gate while maintaining adiabatic evolution or increase the fidelity while keeping the gate time low. The goal of this chapter is to extend an approach presented by Tim Ehret [15] who discussed CD driving for the adiabatic CZ gate by Saffman et al. [23], presented in section 2.3. After that, we find a way to implement E-CD driving for said protocol, show how it can enhance the gate, and test it for its stability. Finally, we implement the proposed gate in an error correction circuit and end with a discussion on a modified protocol that uses only single-qubit terms.

3.1 CD driving

A possibility to use CD driving for the adiabatic CZ gate was discussed by Tim Ehret [15, pp. 19-23]. While the system is highly degenerated, it turns out that it can be factorized into five subsystems. As such, the degeneracy does not cause any problems in this case and it is valid using the formula for the counterdiabatic Hamiltonian from (2.27).

Avoiding the unwanted dynamical phase using CD driving

The protocol suggested by Saffman et al. produces the CZ gate by making use of dynamical and geometric phases, generated by the Gaussian-like pulses. We pointed out before that due to an imperfect Rydberg blockade a small unwanted dynamical phase $\phi_r \propto T_{\text{tot}}/V$ is generated in state $|11\rangle$, which decreases the fidelity of superposition states. From the approximated expression one can see that the dynamical phase can be rendered arbitrarily small by making use of CD driving and accelerating the protocol.
If one has access to CD driving, one might even go further and use only the CD Hamiltonian without the original Hamiltonian H_0 (except for the Rydberg blockade part). This corresponds to switching off the pulses Δ and Ω so that only $H_{\text{CD}} + H_V$ acts on the system where $H_V =$

$V|rr\rangle\langle rr|$. The CD Hamiltonian reproduces the same geometric phase in $|11\rangle$ as the original Hamiltonian, but not the dynamical phase. Depending on the system this might be an undesired effect, however, in our case, it solves the unwanted phase problem completely. A quantitative comparison of this effect is discussed in section 3.2.

Significant matrix elements

It was pointed out by Ehret before that only several entries of H_{CD} contribute to the time evolution of the states [15, pp. 21-23]. This can be seen when visualizing the maximum absolute values of the entries of H_{CD} (see Fig. 3.1). It can be concluded that for high Rydberg blockades only the elements driving the transitions $|01\rangle \leftrightarrow |0r\rangle$, $|10\rangle \leftrightarrow |r0\rangle$, $|11\rangle \leftrightarrow |r1\rangle$ and $|11\rangle \leftrightarrow |1r\rangle$ contribute significantly. A quantitative test of this assumption can be found in Fig. 3.2 by comparing the difference in fidelity between using the full CD Hamiltonian or only the 8 mentioned significant entries. In the following, we will also show this result analytically.

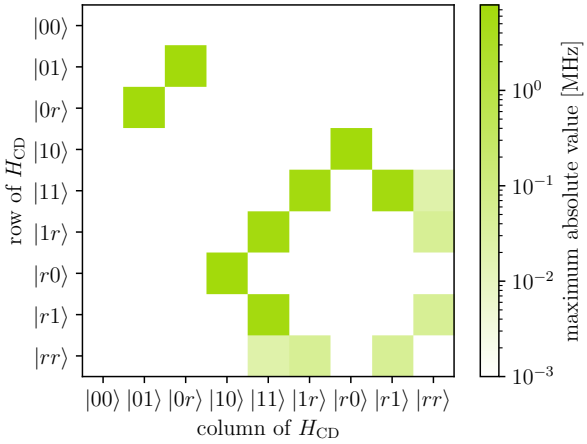

Figure 3.1: Visualization of the matrix entries of H_{CD}. Shown is the maximum absolute value of each element during the protocol. The values for T, $\Omega_{\max}$ and $\Delta_{\max}$ are the same as in the Saffman paper. The Rydberg blockade is chosen to be $V = 10^4$ MHz.

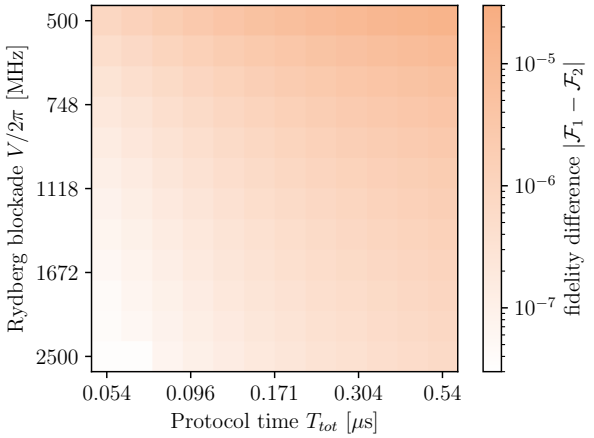

Figure 3.2: Difference between the fidelity using the full H_{CD} without H_0 ($\mathcal{F}_1$) and after reducing it to the 8 significant entries ($\mathcal{F}_2$). The parameters T, $\Omega_{\max}$ and $\Delta_{\max}$ are again the same as in the paper. The initial state was $(|00\rangle+|11\rangle)/\sqrt{2}$.

Analytical derivation of the CD Hamiltonian

Before we turn to high Rydberg blockades, it is worth briefly looking at the case $V = 0$. Without any interaction, the Hamiltonian H_0 separates into two uncoupled systems that resemble shifted

Landau-Zener systems. One may therefore check that H_0 is diagonalized by

$$U = \begin{pmatrix} 1 & 0 & 0 \\ 0 & -\sin\theta & \cos\theta \\ 0 & \cos\theta & \sin\theta \end{pmatrix} \otimes \begin{pmatrix} 1 & 0 & 0 \\ 0 & -\sin\theta & \cos\theta \\ 0 & \cos\theta & \sin\theta \end{pmatrix} \tag{3.1}$$

where $\theta = \frac{1}{2}\arctan(-\Omega/\Delta)$. The counterdiabatic Hamiltonian can be obtained by using $H_{\mathrm{CD}} = i\dot{U}U^\dagger$

$$H_{\mathrm{CD}} = -i\left[\begin{pmatrix} 0 & 0 & 0 \\ 0 & 0 & \dot{\theta} \\ 0 & -\dot{\theta} & 0 \end{pmatrix} \otimes \mathbb{1} + \mathbb{1} \otimes \begin{pmatrix} 0 & 0 & 0 \\ 0 & 0 & \dot{\theta} \\ 0 & -\dot{\theta} & 0 \end{pmatrix}\right]. \tag{3.2}$$

This confirms that in the $V = 0$ case the problem indeed just separates into two Landau-Zener systems.

Turning to the case $V \to \infty$, it will be beneficial to express H_0 in the basis $\{|00\rangle, |01\rangle, |0r\rangle, |10\rangle, |r0\rangle, \frac{1}{\sqrt{2}}(|1r\rangle - |r1\rangle), |11\rangle, \frac{1}{\sqrt{2}}(|1r\rangle + |r1\rangle), |rr\rangle\}$, where the system decomposes into five subsystems of which the largest has dimensions 3×3

$$H_0 = \frac{1}{2}\begin{pmatrix} 0 & & & & & & & & \\ & 0 & \Omega & & & & & & \\ & \Omega & 2\Delta & & & & & & \\ & & & 0 & \Omega & & & & \\ & & & \Omega & 2\Delta & & & & \\ & & & & & \Delta & & & \\ & & & & & & 0 & \sqrt{2}\Omega & 0 \\ & & & & & & \sqrt{2}\Omega & 2\Delta & \sqrt{2}\Omega \\ & & & & & & 0 & \sqrt{2}\Omega & 4\Delta + 2V \end{pmatrix}. \tag{3.3}$$

Two of the three subsystems with off-diagonal elements resemble Landau-Zener-Systems for which we know the terms that appear in H_{CD}. Hence, the problem reduces to calculating the counterdiabatic Hamiltonian of the bottom right 3×3 matrix. Alternatively one may argue that only eigenvectors, that change when varying V, are the ones belonging to the 3×3 matrix in the bottom right corner. Therefore the other entries of H_{CD} can later also be taken from the $V = 0$ case.

Since the matrix is only 3×3, the eigenvectors could be calculated directly without any approximation. We tried to do this, but the resulting terms quickly got very large and hard to work with. Since the gate already operates in the regime of high Rydberg blockades it will prove

sufficient and more convenient to restrict to $V \to \infty$. This motivates us to follow a perturbative approach by rewriting

$$\begin{pmatrix} 0 & \sqrt{2}\Omega & 0 \\ \sqrt{2} & 2\Delta & \sqrt{2}\Omega \\ 0 & \sqrt{2}\Omega & 4\Delta + 2V \end{pmatrix} =: V\left(H_0 + \frac{1}{V}H_1\right) \tag{3.4}$$

The eigenvectors of the 3×3 matrix can be calculated by writing down and solving the eigenvalue equation in first order $1/V$. The result is

$$\{v\} = \left\{ \begin{pmatrix} -\sin\theta' \\ \cos\theta' \\ -\nu\cos\theta' \end{pmatrix}, \begin{pmatrix} \cos\theta' \\ \sin\theta' \\ -\nu\sin\theta' \end{pmatrix}, \begin{pmatrix} 0 \\ \nu \\ 1 \end{pmatrix} \right\} \tag{3.5}$$

(see A.2 for the detailed calculation), where we defined

$$\theta' = \frac{1}{2}\arctan\left(\sqrt{2}\frac{\Omega}{\Delta}\right), \qquad \nu = \frac{\Omega}{\sqrt{2}V}. \tag{3.6}$$

The vectors are normalized up to the first order in $1/V$. As we did before, we can construct a matrix U from the eigenvectors that diagonalizes the 3×3 Hamiltonian. The CD Hamiltonian for the submatrix can then be easily determined using again

$$i\dot{U}U^\dagger = \begin{pmatrix} 0 & -i\dot{\theta}' & 0 \\ i\dot{\theta}' & 0 & 0 \\ 0 & 0 & 0 \end{pmatrix} + \mathcal{O}\left(\frac{1}{V}\right) \tag{3.7}$$

The same result can be produced by adiabatically eliminating the $|rr\rangle$ state and finding that the remaining system is essentially a Landau-Zener system. To return to the full 9×9 basis we have to include the terms of the CD Hamiltonian acting on the other subsystems. As said before this includes only two Landau-Zener subsystems for which we know the solution. Thus

the full CD Hamiltonian reads

$$H_{\mathrm{CD}} = -i \begin{pmatrix} 0 & & & & & & & & \\ & 0 & \dot{\theta} & & & & & & \\ & -\dot{\theta} & 0 & & & & & & \\ & & & 0 & \dot{\theta} & & & & \\ & & & -\dot{\theta} & 0 & & & & \\ & & & & & 0 & & & \\ & & & & & & 0 & \dot{\theta}' & \\ & & & & & & -\dot{\theta}' & 0 & \\ & & & & & & & & 0 \end{pmatrix}. \tag{3.8}$$

Recall that this is in the basis including superposition states. Going back to the computational basis $\{|0\rangle, |1\rangle, |r\rangle\} \otimes \{|0\rangle, |1\rangle, |r\rangle\}$, the CD Hamiltonian takes the form

$$H_{\mathrm{CD}} = -i \left[\dot{\theta} \big(|01\rangle\langle 0r| + |10\rangle\langle r0| \big) + \frac{\dot{\theta}'}{\sqrt{2}} \big(|11\rangle\langle 1r| + |11\rangle\langle r1| \big) \right] + \mathrm{h.c.} \tag{3.9}$$

This is the exact form mentioned at the beginning of the chapter: in the limit of large V only 8 significant matrix elements appear in the Hamiltonian. It is not surprising that all elements affecting the $|rr\rangle$ state vanish, since in the limit we discussed the bandwidth is so large that the population of this state is negligible. For sake of convenience, we may also rewrite (3.9) as

$$H_{\mathrm{CD}} = f_1(P_0 \otimes \sigma_y + \sigma_y \otimes P_0) + f_2(P_1 \otimes \sigma_y + \sigma_y \otimes P_1), \tag{3.10}$$

where we defined the functions $f_1(t) := \dot{\theta}(t)$ and $f_2(t) := \dot{\theta}'(t)/\sqrt{2}$ and the projectors $P_0 := |0\rangle\langle 0|$, $P_1 := |1\rangle\langle 1|$ and $P_r := |r\rangle\langle r|$. The matrix denoted as σ_y is a Pauli y-matrix in the basis $\{|1\rangle, |r\rangle\}$ so in this case what is really meant is

$$\sigma_y = \begin{pmatrix} 0 & 0 & 0 \\ 0 & 0 & -i \\ 0 & i & 0 \end{pmatrix}. \tag{3.11}$$

The remaining H_{CD} is characterized only by the two functions $f_1 = \dot{\theta}$ and $f_2 = \dot{\theta}'/\sqrt{2}$. Inserting the definitions of θ and θ', they can be identified as

$$f_1 = \frac{1}{2}\frac{\Omega\dot{\Delta} - \dot{\Omega}\Delta}{\Delta^2 + \Omega^2}, \qquad f_2 = \frac{1}{2}\frac{\Omega\dot{\Delta} - \dot{\Omega}\Delta}{\Delta^2 + 2\Omega^2}. \tag{3.12}$$

Naturally, one may also extract these functions as a result of calculating H_{CD} numerically after choosing a large value for V. When we compared the functions deducted via the two methods, the analytical and numerical f_1 were identical up to numerical precision, while between f_2 and its numerical counterpart, we get a difference that falls off with $1/V$. For the specific pulses of the adiabatic CZ gate, the functions are visualized in Fig. 3.3. As can be seen from the algebraic form, the functions differ the most at the points where the detuning Δ reaches zero, at which points $f_1 = 2f_2$. This will play a more important role later on when trying to construct an E-CD Hamiltonian using single-qubit terms in section 3.5.

3.2 E-CD driving of the adiabatic CZ gate

In the previous section, we discussed that the counterdiabatic Hamiltonian for the adiabatic CZ gate may be approximated as (3.10) in the limit of high Rydberg blockades. This Hamiltonian is purely imaginary, which makes it difficult to realize experimentally. We already presented a solution to this problem in the introduction, namely by using effective counterdiabatic driving. The main contribution of this thesis will be to apply this method to the adiabatic CZ gate in order to increase fidelity and reduce gate times. To do so, we have to find an ansatz for H_{E} that can emulate the CD Hamiltonian. A suitable choice will turn out to be

$$H_E = \sqrt{\omega}\left[c_1(\sigma_x \otimes P_0 + P_0 \otimes \sigma_x) + c_2(\sigma_x \otimes P_1 + P_1 \otimes \sigma_x) + c_3(P_r \otimes \mathbb{1} + \mathbb{1} \otimes P_r)\right] \tag{3.13}$$

with the c_i defined as in (2.36) and with σ_x a Pauli x matrix, again in the basis $\{|1\rangle, |r\rangle\}$

$$\sigma_x = \begin{pmatrix} 0 & 0 & 0 \\ 0 & 0 & 1 \\ 0 & 1 & 0 \end{pmatrix}. \tag{3.14}$$

In order to anticipate a further discussion we want to note that this Hamiltonian is still challenging to realize experimentally since it contains two-qubit terms that do not allow to apply lasers on one atom independent of the state of the other. We will discuss this issue and a possible

workaround in section 3.5. Choosing the Fourier series of the c_i in (2.36) to be of first order $L = 1$, the condition $M^{(1)}_{\mathrm{CD}}(T) = M^{(2)}_{\mathrm{E}}(T)$ becomes

$$A_{11}B_{31} - B_{11}A_{31} = 2f_1, \qquad A_{21}B_{31} - B_{21}A_{31} = 2f_2 \tag{3.15}$$

(see A.3 for the calculation). A possible solution is

$$\begin{aligned} A_{11} &= \sqrt{2|f_1|}, & B_{31} &= \mathrm{sgn}(f_1)\sqrt{2|f_1|}, \\ B_{21} &= \sqrt{2|f_2|}, & A_{31} &= -\mathrm{sgn}(f_2)\sqrt{2|f_2|}, \end{aligned} \tag{3.16}$$

and $B_{11} = A_{21} = 0$, such that the coefficients read

$$\begin{aligned} c_1 &= A_{11}\sin(\omega t), \\ c_2 &= B_{21}\cos(\omega t), \\ c_3 &= A_{31}\sin(\omega t) + B_{31}\cos(\omega t). \end{aligned} \tag{3.17}$$

We can now use this effective CD Hamiltonian to emulate CD driving on the two Rydberg atoms. However, one should keep in mind that the driving frequency ω has to be chosen sufficiently large.

Modifying the pulse shape

In the previous sections, we derived the functional form of f_1 and f_2 that make up H_{CD}. We can see in Fig. 3.3 that these functions are not continuous, since the time derivative of the Rabi pulse $\dot{\Omega}$ is not continuous. This can raise problems if we try to use these functions for E-CD driving. Therefore we aim to modify the Rabi pulse, such that the derivative is also continuous. The pulses we have used so far are essentially Gaussian pulses of the form

$$\Omega(t) = \frac{\Omega_{\max}}{\mathcal{N}}\left[\exp\left(-\frac{(t - T/2)^4}{\tau^4}\right) - a\right]. \tag{3.18}$$

With the scaling factor $\mathcal{N} = 1 - a$ such that $\Omega_{\max} = \max\{\Omega(t)\}$. Since the second pulse is the same as the first one just shifted by $T/2 + T_2$, it will suffice to treat only the first pulse here. The offset a is included so that one may impose $\Omega(0) = \Omega(T/2) = 0$ for the first pulse. To make the derivative continuous, we further need to impose $\dot{\Omega}(0) = \dot{\Omega}(T/2) = 0$. This condition requires at least adding a term quadratic in t so that the pulse remains symmetric, which leads

to the ansatz

$$\Omega_{\text{mod.}}(t) = \frac{\Omega_{\max}}{\mathcal{N}} \left[\exp\left(-\frac{(t - T/4)^4}{\tau^4} \right) - a - bt\left(t - \frac{T}{2} \right) \right]. \tag{3.19}$$

Taking the derivative and imposing the aforementioned boundary conditions yields

$$a = \exp\left(-\frac{(T/4)^4}{\tau^4} \right), \qquad b = \frac{T^2}{8\tau^4} a. \tag{3.20}$$

The normalization factor $\mathcal{N}$ can be determined numerically to give $\max\{\Omega_{\text{mod.}}(t)\} = \Omega_{\max}$. In the following, we will use these modified pulses for the E-CD driving since they produced better results in general.

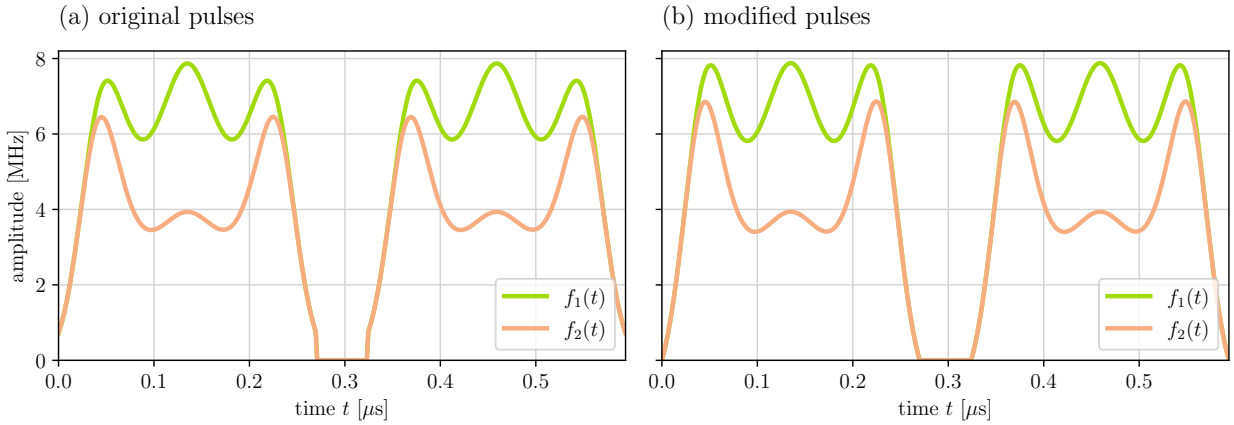

Figure 3.3: (a) Visualization of the two functions that constitute the CD Hamiltonian in the limit $V \to \infty$. The parameters are the same as in the original paper. (b) Visualization of the functions for the modified Rabi pulse and detuning. By modifying the pulses we were able to get rid of the jumps at the beginning and the end of each pulse.

Fidelity improvements by E-CD driving

Having completed the theoretical part behind the E-CD driving for the adiabatic CZ gate, we can look at the numerics to test in which parameter regimes the E-CD driving can improve the fidelity. The adiabatic gate proposed by Saffman et al. [23] works perfectly for large Rydberg blockades in the adiabatic limit i.e. for arbitrarily long times or large pulses. If one has experimental access only to smaller pulses and a finite Rydberg blockade, non-adiabatic errors affect the fidelity of the gate and corrections are necessary. In Fig. 3.4 we compare the fidelities with the input state $(|00\rangle + |11\rangle)/\sqrt{2}$ using several different methods to recreate a CZ gate: (a) the original Hamiltonian as proposed by Saffman et al., (b) the original Hamiltonian

with E-CD driving and (c) only the E-CD Hamiltonian. We further show what results one could get, having access to (d) the original Hamiltonian with CD driving or (e) only the CD Hamiltonian.

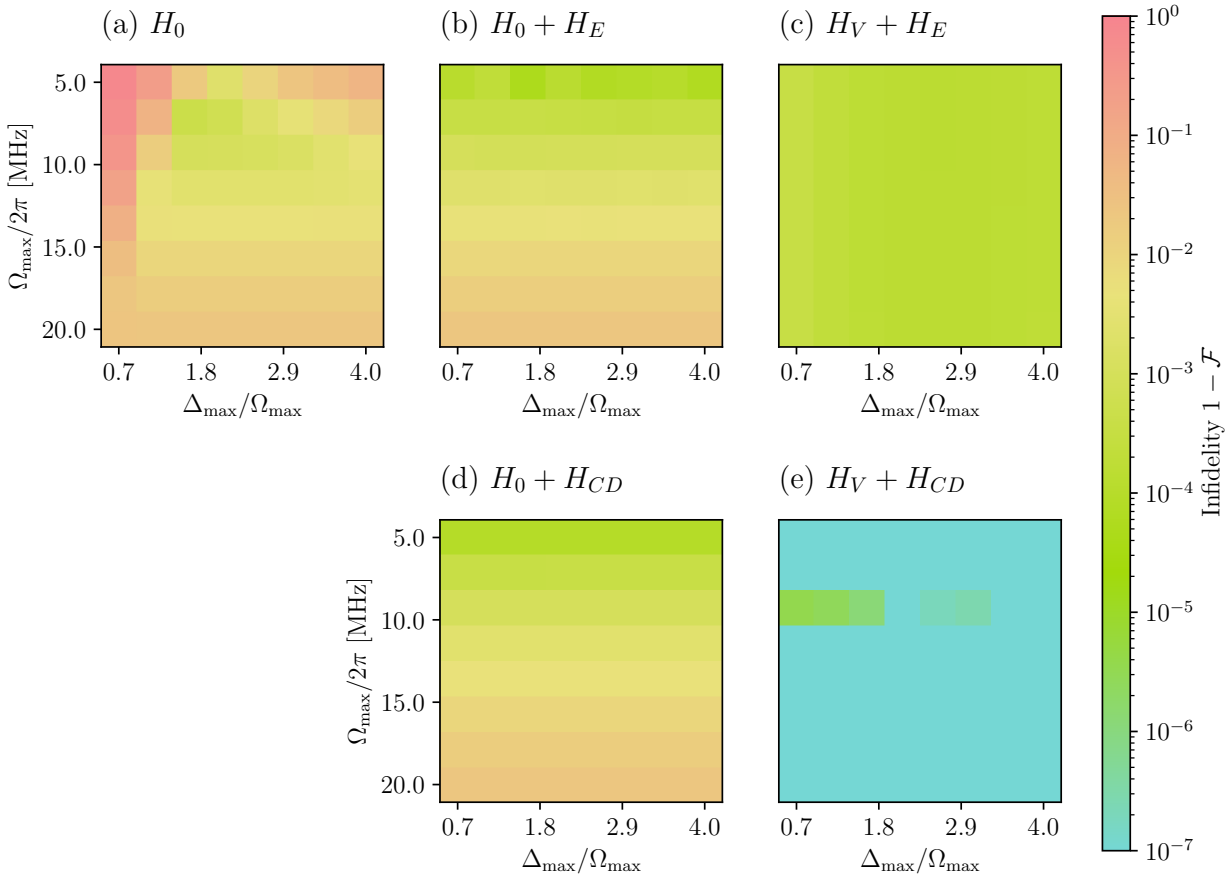

Figure 3.4: Infidelity of state $|00\rangle + |11\rangle$ for different variations of the adiabatic CZ gate as discussed in the text. The parameters were $T = 0.54\,\mu$s, $V/2\pi = 800$ MHz and $\omega = 300$ MHz.

The original protocol performs well around the parameters used in the original paper of $\Omega_{\max}/2\pi = 17$ MHz and $\Delta_{\max}/2\pi = 23$ MHz with infidelities $< 10^{-3}$. Smaller Rabi pulses and lower detuning cause diabatic errors that can be corrected using E-CD driving. For larger pulses, the error is dominated by the unwanted dynamical phase. This issue cannot be avoided by adding H_{E} or H_{CD} as can be seen from (b) and (d). As discussed previously, setting Δ and Ω to zero without changing the counterdiabatic driving solves this issue as can be seen in (c) and (e). It thus appears that the E-CD driving works well for correcting errors due to non-adiabaticity and avoiding the phase error.

Although these results might look good, we have to be careful with this reasoning. Fidelity improvement by counterdiabatic driving usually comes at the expense of having to use large

pulses. This is even more true for effective CD driving, which uses pulses proportional to the square root of the E-CD frequency ω, which again has to be chosen large enough to produce high-fidelity results. It would therefore be a better evaluation to discuss the results after limiting the maximum pulse height of the E-CD Hamiltonian. A brief analysis under this viewpoint can be found in A.4. However, we would now like to slightly shift the focus of our argument and analyze how the presented methods can be used to accelerate the CZ gate.

Acceleration of the gate

In general, using E-CD driving to improve the fidelity or reduce the gate time comes down to the same physics. When accelerating the protocol, the evolution of the states becomes less adiabatic and the fidelity decreases. This is the same as what happens when keeping the gate time constant and reducing the pulse height. We can see this better by taking a closer look at the Schrödinger equation: rescaling the time as $t \to t/s$, the Schrödinger equation scales as

$$i\partial_t|\psi\rangle = H|\psi\rangle \to is\partial_t|\psi\rangle = H|\psi\rangle. \tag{3.21}$$

If the Hamiltonian is also rescaled as $H \to sH$, the dynamics of the system do not change. In other words, accelerating the protocol time is equivalent to amplifying the Hamiltonian. While the Rydberg interaction can be made rather large, it is still experimentally limited and the Hamiltonian cannot be rescaled arbitrarily. If one tries to increase pulses in order to keep the fidelity high for lower gate times, but not the Rydberg interaction, one eventually reaches a limit where $\Omega, \Delta \sim V$ and the process is not adiabatic anymore. Thus, the feasible protocol time is limited when having access to finite Rydberg blockades as can also be seen in Fig. 3.5. Using the parameters from the original paper, accelerating the protocol by a factor of 2-3 produces fidelities < 0.9 for all Rydberg interaction strengths $V/2\pi < 1000$ MHz, even after rescaling the pulses accordingly. E-CD driving corrects for these diabatic errors, producing higher fidelities as long as the E-CD frequency ω is chosen large compared to the protocol time. For $\omega = 300$ MHz we get fidelities > 0.99 for accelerations up to a factor of 3 and > 0.9 for acceleration by a factor of 20.

In conclusion, the E-CD-based CZ gate allows avoidance of errors due to diabatic evolution for lower protocol times or low Rydberg interactions. It provides an advantage over the CZ gate proposed by Saffman et al. [23] when working with medium to high Rydberg Blockades and smaller protocol times at the expense of needing fast oscillating lasers.

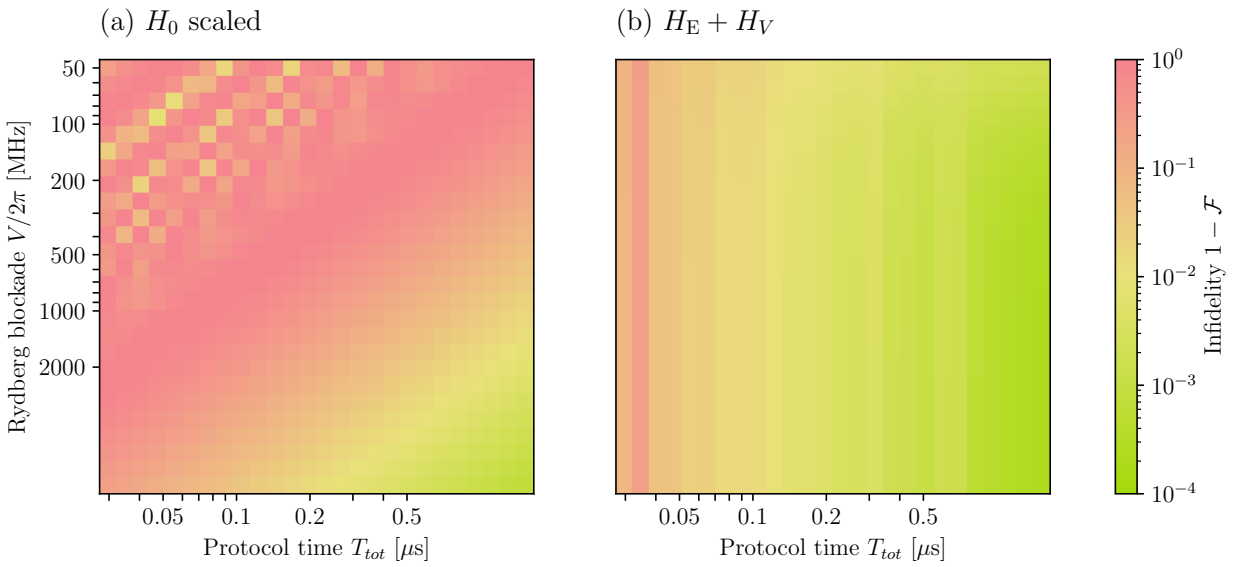

Figure 3.5: (a) Infidelity of the CZ gate as proposed by Saffman et al. using only H_0. The Rabi pulse Ω and the detuning Δ are scaled inverse proportional to the total protocol time T_{tot}. (b) Infidelity using the ECD-driven CZ gate $H_E + V|rr\rangle\langle rr|$. The E-CD frequency is $\omega/2\pi = 300$ MHz

3.3 Stability analysis

Static amplitude errors

In experimental setups, the pulses used to produce the gate will be subject to errors that cannot be controlled. We can test the stability of the protocol under such errors by introducing a small relative error ε. First, we will test the protocol for small errors in the amplitude by replacing

$$\begin{aligned} f_1(t) &\to f_1(t)(1+\varepsilon) \\ f_2(t) &\to f_2(t)(1+\varepsilon). \end{aligned} \tag{3.22}$$

As can be seen in Fig. 3.6 the fidelity appears as a quadratic function with its maximum at $\varepsilon \neq 0$. Similar observations have already been made and discussed in more detail in [41]. The most likely explanation for this effect is that the amplitude error somehow compensates for non-adiabatic errors. This is also in accordance with the stability curves of the accelerated protocol in Fig. 3.6b. Smaller times increase fidelity loss due to non-adiabaticity. Therefore the relative error ε has to be larger in order to compensate for these errors and the maximum gets shifted.

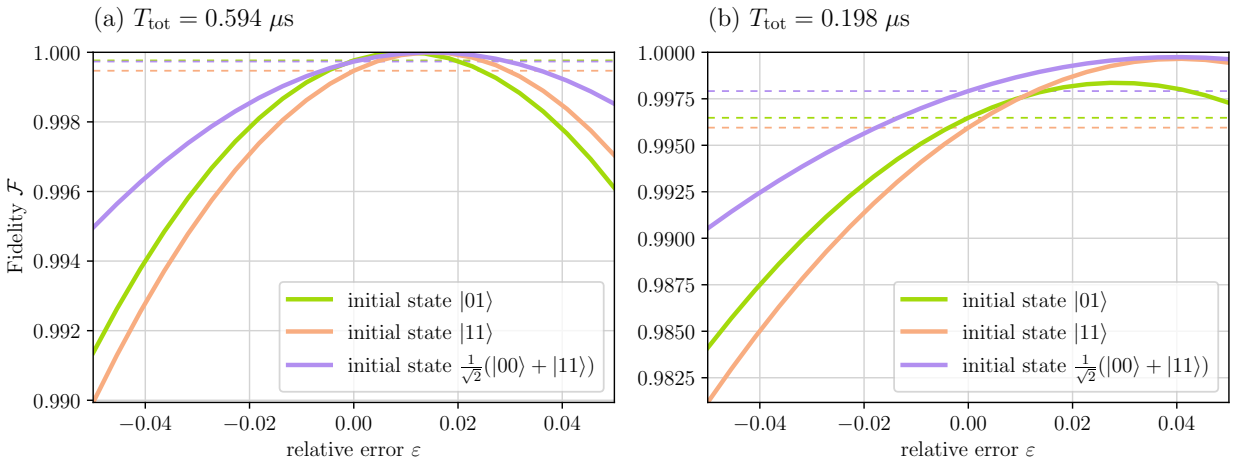

Figure 3.6: Stability of the CZ gate for different input states for (a) $T_{\text{tot}} = 0.594\ \mu$s and (b) $T_{\text{tot}} = 0.198\ \mu$s. The dashed lines show the fidelity at $\varepsilon = 0$. The Rydberg blockade was $V/2\pi = 200$MHz and the E-CD frequency $\omega = 300$ MHz.

In our case, the process is not perfectly adiabatic because we work with a finite E-CD frequency ω. Increasing ω reduces non-adiabaticity and thus shifts the maximum of the stability function towards $\varepsilon = 0$ as can be seen in Fig. 3.7a.

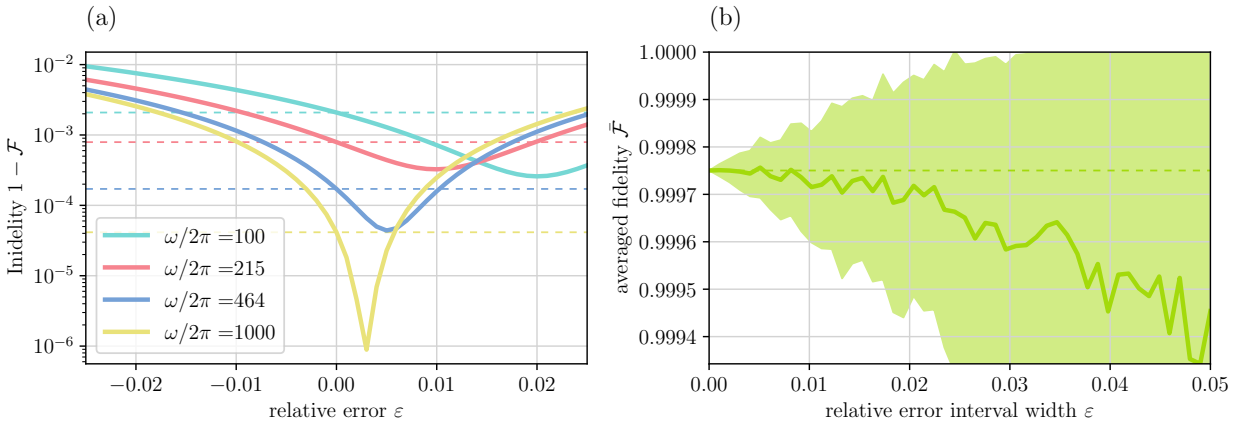

Figure 3.7: (a) Stability of the CZ gate for different E-CD frequencies. The input state was $(|00\rangle + |11\rangle)/\sqrt{2}$. (b) Stability curve of the CZ gate as the arithmetic mean of 100 random errors from the interval $[-\varepsilon/2, \varepsilon/2]$. The shaded area is the variance of the fidelities, the dashed lines show the fidelity at $\varepsilon = 0$.

In a realistic experimental setup, the error ε is not fixed but rather fluctuates within a given error interval $[-\varepsilon/2, \varepsilon/2]$. We simulate such variations by taking $N = 100$ random values from the interval and averaging the fidelity. The result can be found in Fig. 3.7b. As can be seen, the variance appears relatively large. This is due to the fact that the stability curve as in the

previous Fig. 3.6 is anti-symmetric, such that small $\varepsilon > 0$ increase the fidelity while small $\varepsilon < 0$ decrease it. On average, the fidelity decreases by about 0.4% with an upper error boundary of $\pm 2.5\%$. We can conclude that our protocol is stable with regard to small errors on the pulses.

Phase errors

For the E-CD driving, fast oscillating functions are needed. It makes sense to test the stability with regard to relative phase errors between the sine and cosine functions included in the Hamiltonian. In particular, we shift the cosine by a small phase δ

$$\begin{aligned} c_1(t) &= A_{11}\sin(\omega t) \rightarrow A_{11}\sin(\omega t) \\ c_2(t) &= B_{21}\cos(\omega t) \rightarrow B_{21}\cos(\omega t + \delta) \\ c_3(t) &= A_{31}\sin(\omega t) + B_{31}\cos(\omega t) \rightarrow A_{31}\sin(\omega t) + B_{31}\cos(\omega t + \delta). \end{aligned} \tag{3.23}$$

The results can be seen in Fig. 3.8. Contrary to the previous analysis, here the error is symmetric around $\varepsilon = 0$. Looking at a larger interval, one could also see that the stability curve is 2π periodic and has its minima at $\delta = n\pi$ as we would expect from the 2π periodicity of the cosine. A phase error of ± 0.15 decreases the fidelity by 2-6% depending on the input state. This is still a good result regarding the stability of the gate.

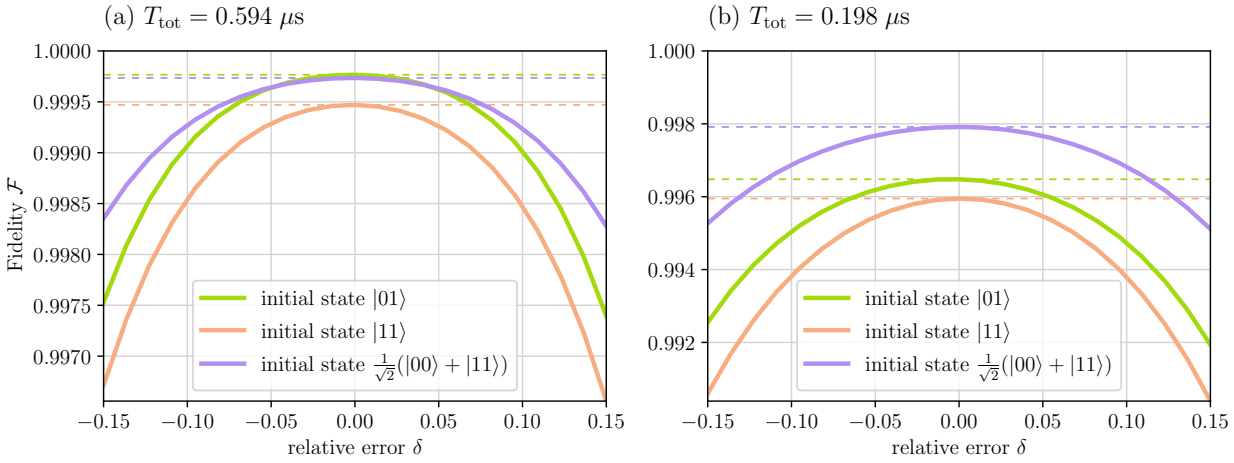

Figure 3.8: Stability of the CZ gate under a relative phase error for (a) $T_{\text{tot}} = 0.594\ \mu$s and (b) $T_{\text{tot}} = 0.198\ \mu$s. The dashed lines show the fidelity at $\varepsilon = 0$. The parameters are the same as in Fig. 3.6

In conclusion, we were able to show that the E-CD-based CZ gate is stable with regard to pulse area errors as well as relative phase errors on the lasers. Accelerating the gate lowers the fidelity

but still produces stable results.

3.4 Quantum error correction

The discussion around the CZ gate so far only makes sense if it can also be well implemented into quantum circuits. We already presented a way to extend the CZ gate to a CNOT gate using single qubit pulses. This section is dedicated to testing this CZ-based CNOT gate in a simple quantum error correction (QEC) circuit, assuming that we have access to perfect single-qubit operations.

Noise is a problem that can occur in quantum computers as much as it does in classical computers. Examples are faulty gate operations or errors that occur due to decoherence. Classical computers can deal with noise by copying bits and encoding the information in more than the minimum bits needed to make the information more robust. In quantum mechanics, the no-cloning-theorem forbids us to directly duplicate qubits [2, pp. 530-531]. However, it is still possible to add redundant information to protect the information stored in qubits from noise.

A simple QEC circuit that corrects for potential unwanted bit flips is presented in [2, pp. 426-429] and [42, pp. 296-297]. The circuit starts with the qubit we are interested in (we call it qubit A), in state $|x\rangle = a|0\rangle + b|1\rangle$. Furthermore, we use two auxiliary qubits (B and C) each starting in state $|0\rangle$. We can break down the protocol into the following steps.

(a) Apply two CNOT gates to entangle the qubits in state $a|000\rangle + b|111\rangle$.

(b) Some perturbation of the system may cause an unwanted bit flip in qubit A, such that the system is now in a state $\alpha(a|000\rangle + b|111\rangle) + \beta(a|100\rangle + b|011\rangle)$, where β is the amplitude of the unwanted state. We simulate this by manually flipping this qubit.

(c) Again apply two CNOT gates. One can show that then the system is in state $(a|0\rangle + b|1\rangle)\alpha|00\rangle + (a|1\rangle + b|0\rangle)\beta|11\rangle$.

(d) Measure the state of the auxiliary qubits B and C. If these qubits are in state $|11\rangle$ flip qubit A, otherwise do nothing.

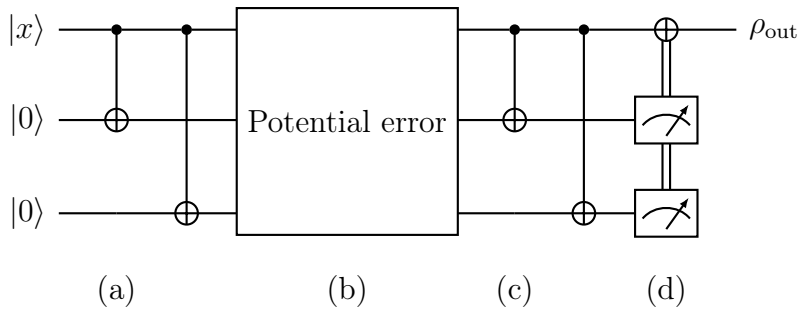

After applying the protocol, qubit A is again in state $|x\rangle$, regardless if a flip occurred or not. In our computations, we implement the protocol by calculating

$$|\psi_{\text{out}}\rangle = \text{NOT} \cdot \text{CNOT}_{\text{AC}} \cdot \text{CNOT}_{\text{AB}} \cdot (\text{flip}) \cdot \text{CNOT}_{\text{AC}} \cdot \text{CNOT}_{\text{AB}} |\psi_{\text{in}}\rangle \tag{3.24}$$

and tracing out systems B and C to obtain the density matrix representing the final state of qubit A $\rho_{\text{out}} = \text{Tr}_{B,C}(|\psi_{\text{out}}\rangle\langle\psi_{\text{out}}|)$. The NOT gate flips qubit A, if qubit B and C are in state $|11\rangle$. The fidelity is then calculated via

$$\mathcal{F} = \langle x|\rho_{\text{out}}|x\rangle. \tag{3.25}$$

The results can be found in table 3.1. We could also include a potential bitflip on qubit B or C instead of A. However, this produces the same fidelity as no bit flip at all, since in the end only the fidelity of qubit A is measured and it does not make a difference for the protocol if only one auxiliary qubit is flipped. In all cases the fidelity is > 0.999, demonstrating that the CZ gate works well when being included in a more complex circuit.

Initial state $\|x\rangle$	Bit flip on qubit A	Fidelity $\mathcal{F}$
$\|0\rangle$	no	0.999254
	yes	0.999403
$\|1\rangle$	no	>0.999999
	yes	0.999126
$\frac{1}{\sqrt{2}}(\|0\rangle + \|1\rangle)$	no	0.999181
	yes	0.999560
$\frac{1}{\sqrt{2}}(\|0\rangle + i\|1\rangle)$	no	0.999181
	yes	0.999190

Table 3.1: Fidelity after of the bitflip QEC circuit using our proposed CNOT gate. The parameters of the CZ gate applied were $T = 0.54$ μs, $\Omega_{\text{max}}/2\pi = 17$ MHz, $\Delta_{\text{max}}/2\pi = 23$ MHz as in the Saffman paper, the Rydberg blockade is $V/2\pi = 200$ MHz and the ECD frequency $\omega/2\pi = 350$ MHz.

A more detailed analysis of how the QEC circuit affects certain input states can be seen in Fig. 3.9, where the difference between input and output density matrices is shown.
We remark that the infidelity of the gate does not increase linearly with the number of CNOT gates included as one would might expect. When applying the gate once, a small population remains in states like $|1r\rangle$ and $|r1\rangle$, which causes the fidelity of the gate to decrease. Because we assume a closed system, this population is not lost so a repeated application of the gate might bring some of the population back into the computational basis states, countering further loss of fidelity. Therefore, the infidelity does not progress trivially and one at least has to be careful drawing general conclusions from the presented example.

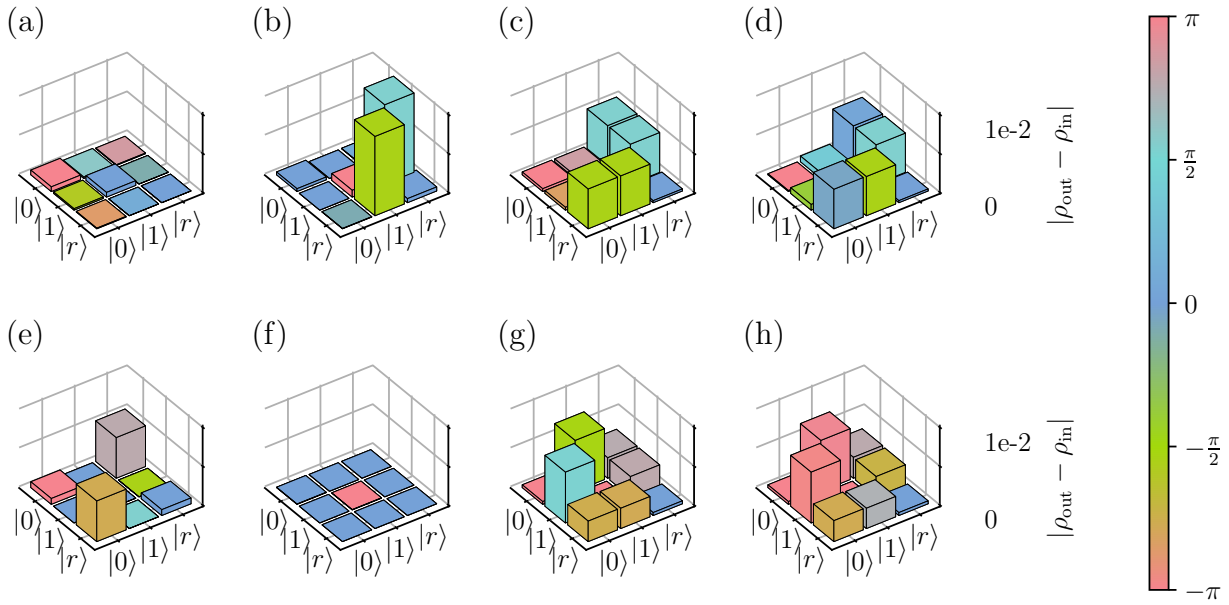

Figure 3.9: Difference between different input density matrices and their output from the QEC circuit. (a-d) show initial states $|0\rangle$, $|1\rangle$, $(|0\rangle + |1\rangle)/\sqrt{2}$ and $(|0\rangle + i|1\rangle)/\sqrt{2}$ without a bitflip. (e-h) show the same results with an unwanted bitflip.

Quantum process tomography

Often the fidelity is not a satisfying quantity to characterize the quality of quantum mechanical processes. Quantum process tomography (QPT) gives a more detailed and state-independent representation of an experimental implementation e.g. of a quantum gate. The basic idea of QPT is to represent the transformation of the density matrix of a process using a set of basis matrices.
The explanation presented here follows [43, pp. 2-3] and [44, pp. 164-166]. Suppose we are

given a process that can be described by a completely positive linear map

$$\mathcal{E}(\rho_{\text{in}}) = \sum_i A_i \rho_{\text{in}} A_i^\dagger \tag{3.26}$$

where ρ_{in} is the initial density matrix and $\{A_i\}$ a set of operators that describe the transformation. Given a set of basis operators $\{B_n\}$, we can write out the map as

$$\mathcal{E}(\rho_{\text{in}}) = \sum_{mn} \chi_{mn} B_m \rho_{\text{in}} B_n^\dagger, \tag{3.27}$$

where now the coefficients χ_{mn} contain the information on how the map transforms density matrices. These coefficients can be interpreted as the entries of a $N^2 \times N^2$ matrix χ. Writing out the density matrix in its vector representation defined by

$$\rho = \sum_{ij} \rho_{ij} |i\rangle\langle j| \rightarrow \tilde{\rho} = \sum_{ij} \rho_{ij} |i\rangle \otimes |j\rangle, \tag{3.28}$$

the action of the linear map on the input density matrix can be expressed using a superoperator U as $\mathcal{E}(\tilde{\rho}) = U\tilde{\rho}_{\text{in}} = \tilde{\rho}_{\text{out}}$. It can be shown that this linear transformation can then be written as

$$\tilde{\rho}_{\text{out}} = U\tilde{\rho}_{\text{in}} = \sum_{mn} \chi_{mn} \tilde{B}_m \tilde{B}_n^\dagger \tilde{\rho}_{\text{in}}. \tag{3.29}$$

Using the vector representation of density matrices, we can determine U and χ (for more details see [44, pp. 164-166]). Since we work with 3 state atoms we need a basis of hermitian 3×3 matrices. Such a basis is given by the Gell-Mann matrices and the unity matrix

$$\begin{aligned}
\lambda_1 &= \begin{pmatrix} 0 & 1 & 0 \\ 1 & 0 & 0 \\ 0 & 0 & 0 \end{pmatrix}, \quad \lambda_2 = \begin{pmatrix} 0 & -i & 0 \\ i & 0 & 0 \\ 0 & 0 & 0 \end{pmatrix}, \quad \lambda_3 = \begin{pmatrix} 1 & 0 & 0 \\ 0 & -1 & 0 \\ 0 & 0 & 0 \end{pmatrix}, \\
\lambda_4 &= \begin{pmatrix} 0 & 0 & 1 \\ 0 & 0 & 0 \\ 1 & 0 & 0 \end{pmatrix}, \quad \lambda_5 = \begin{pmatrix} 0 & 0 & -i \\ 0 & 0 & 0 \\ i & 0 & 0 \end{pmatrix}, \quad \lambda_6 = \begin{pmatrix} 0 & 0 & 0 \\ 0 & 0 & 1 \\ 0 & 1 & 0 \end{pmatrix}, \\
\lambda_7 &= \begin{pmatrix} 0 & 0 & 0 \\ 0 & 0 & -i \\ 0 & i & 0 \end{pmatrix}, \quad \lambda_8 = \frac{1}{\sqrt{3}} \begin{pmatrix} 1 & 0 & 0 \\ 0 & 1 & 0 \\ 0 & 0 & -2 \end{pmatrix}, \quad I = \begin{pmatrix} 1 & 0 & 0 \\ 0 & 1 & 0 \\ 0 & 0 & 1 \end{pmatrix}.
\end{aligned} \tag{3.30}$$

We can treat the whole QEC circuit as a linear map acting on the density operator $\rho_{\text{in}} = |x\rangle\langle x|$. The result of the process tomography for the E-CD-based QEC circuit compared to an ideal QEC circuit can be seen in Fig. 3.10

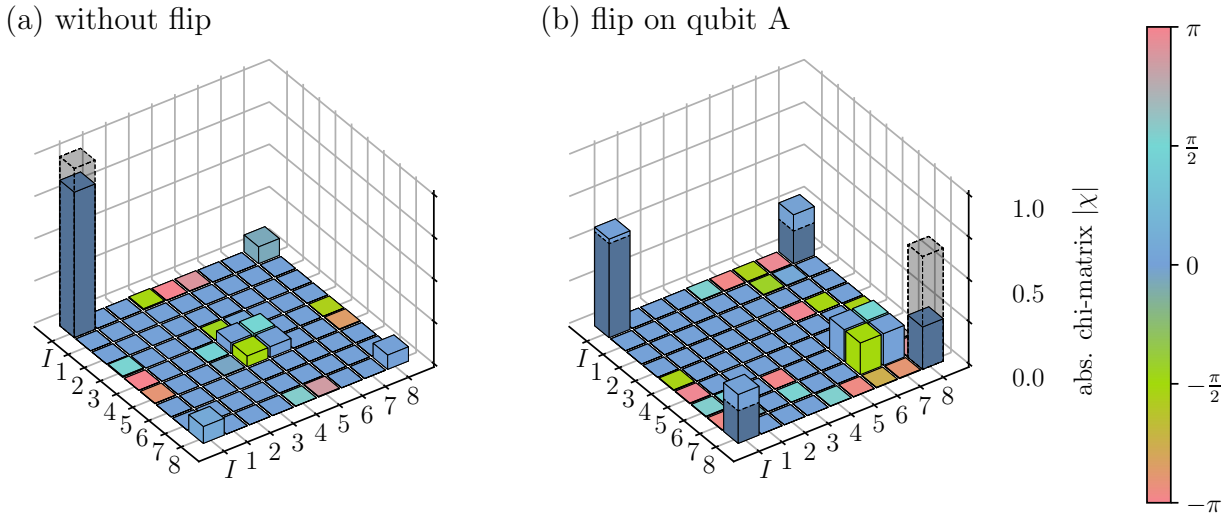

Figure 3.10: Quantum tomography for the QEC circuit without (a) and with (b) an accidental flip of qubit A and the Gell-Mann matrices as the basis. The transparent bars show the result obtained using a perfect CZ gate. The parameters were the same as in Fig. 3.9.

3.5 Using single qubit Hamiltonians for the E-CD driving

The major issue of the method presented so far is the fact that the proposed Hamiltonian for E-CD driving in (3.13) uses two-qubit terms that are difficult to realize in real systems. An experimentally feasible E-CD Hamiltonian should have the form $H_E = M \otimes \mathbb{1} + \mathbb{1} \otimes M$, acting on one system independent of the other. Making such an Ansatz for the E-CD Hamiltonian heavily restricts us, so much that it turns out to be difficult to find a proper solution.
The problem can be made easier by making two assumptions. The first of which is assuming $f_1 \approx \bar{f} \approx f_2$ for the functions in the CD Hamiltonian in (3.10). We can for example take $\bar{f}$ to be the arithmetic mean of f_1 and f_2. The second assumption is that the Rydberg Blockade V is large so that we can add and subtract terms in the Hamiltonian affecting the state $|rr\rangle$ without changing the dynamics of the system. This allows us to write the CD Hamiltonian using single qubit terms

$$H_{\text{CD}} \approx \bar{f}(\sigma_y \otimes \mathbb{1} + \mathbb{1} \otimes \sigma_y). \tag{3.31}$$

One can see that this Hamiltonian has the same form as the one we obtained previously in the case $V = 0$. Using this Hamiltonian and a single-qubit ansatz for the ECD Hamiltonian, we find a possible solution to be

$$H_{\text{E, mean}} = \sqrt{2\omega\bar{f}} \left[\begin{pmatrix} 0 & 0 & 0 \\ 0 & 0 & \sin(\omega t) \\ 0 & \sin(\omega t) & \cos(\omega t) \end{pmatrix} \otimes \mathbb{1} + \mathbb{1} \begin{pmatrix} 0 & 0 & 0 \\ 0 & 0 & \sin(\omega t) \\ 0 & \sin(\omega t) & \cos(\omega t) \end{pmatrix} \right]. \tag{3.32}$$

We have to be careful since the approximation $f_1 \approx f_2$ is not true in general. The analytical form of the functions (3.12) suggests that the approximation is justified in domains where $\Delta \gg \Omega$. Having points where Δ vanishes, as is the case for the adiabatic CZ gate, can lead to problems on the other hand. However, this method can still provide an advantage over the original protocol in some parameter regimes. Our tests revealed that adding this mean-function E-CD Hamiltonian to the original Hamiltonian improves the gate fidelity when accelerating the gate and working in the regime of medium to high Rydberg blockades as can be seen in fig. 3.11.

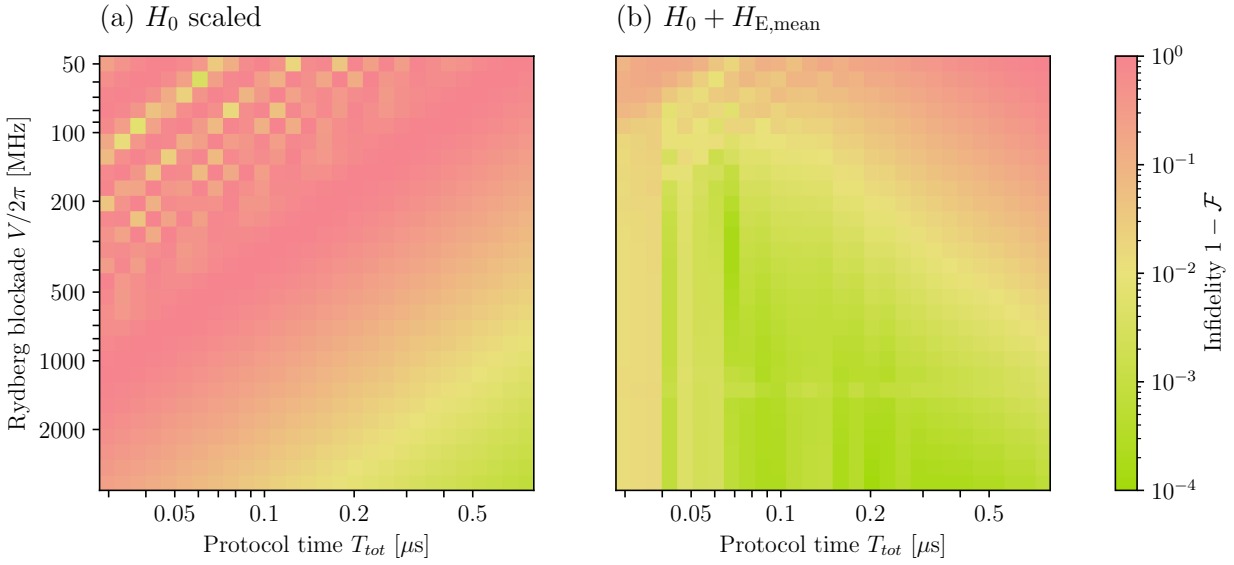

Figure 3.11: (a) Infidelity of the CZ gate as proposed by Saffman et al. using only H_0. The Rabi pulse Ω and the detuning Δ scale inverse proportional to the total protocol time T_{tot}. (b) Infidelity using the E-CD-driven CZ gate $H_0 + H_{\text{E,mean}}$ with the mean function approximation $f_1 \approx f_2$. The E-CD frequency is $\omega/2\pi = 1000$ MHz.

Using $H_{\text{E, mean}}$ without H_0 as done previously did not result in convincing performance of the gate so we will refrain from discussing this case. Because of that, the approach discussed in this section does not avoid the unwanted dynamical phase error. We also need to turn the E-CD

frequency ω higher in order to produce good results. The high-fidelity region in Fig. 3.11b can be explained by the fact that smaller gate times reduce the unwanted phase error as well as higher Rydberg blockades. In general, the mean function approximation is not exact and shows to be more sensitive to the input state and other parameters, than the previously discussed E-CD.

In conclusion, these results show that by modifying the effective counterdiabatic driving to be more feasible for experimental setups, the performance is limited but can still enable us to produce a high-fidelity CZ gate in parameter regimes where this is more difficult for the original protocol. Some of the benefits gained from E-CD driving discussed in section 3.2 still apply in some regimes and hold the potential to improve the gate.

4 Conclusion and outlook

Conclusion

In this thesis, we looked at an implementation of a quantum CZ gate based on cold neutral Rydberg atoms. We started from an approach provided by Tim Ehret [15] who used counterdiabatic driving to enhance an adiabatic CZ gate based on Rydberg atoms proposed by Saffman et al. [23]. We were able to find an analytic expression for the counterdiabatic Hamiltonian in the limit of high Rydberg interactions and showed that it uses two different functions for driving the transitions. Most importantly, we extended the CD approach by working out an effective counterdiabatic (E-CD) Hamiltonian, which can emulate the time evolution of the imaginary CD Hamiltonian using only real, fast-oscillating terms. We showed that the usage of such an effective counterdiabatic Hamiltonian has multiple benefits, ultimately increasing the fidelity of the gate. We saw that in the case of limited Rydberg interactions, the effective CD driving can be utilized to avoid an unwanted dynamical phase error in state $|11\rangle$ that is produced in the original protocol. In addition, E-CD driving allows to reduce the gate times while keeping the process adiabatic, i.e. the fidelity high. We tested the protocol for its stability under relative pulse errors and relative phase errors and showed that it is robust under these variations. Furthermore, we extended the CZ gate into a CNOT gate that could be implemented in a simple quantum error correction circuit and demonstrated that the gate still produces good results after multiple applications. Finally, we addressed the issue that the E-CD approach uses a Hamiltonian, which is difficult to realize experimentally since it contains two-qubit terms. We discussed an experimentally more feasible implementation of the gate which uses only single-qubit terms. While the fidelity of this gate is more sensitive to the parameters used, we were able to demonstrate that a more realistic implementation of the E-CD gate could be feasible.

Technichal issues and outlook

The biggest issue of the E-CD-based CZ gate is the fact that it uses two-qubit terms, which are not very easy to implement in an experimental setup. We discussed one possible approach to solve this, by approximating the functions of the CD Hamiltonian to be equal. The results produced this way do not seem too bad but leave room for improvement. We cannot make use of the full potential of the E-CD driving e.g. by using only H_{E} and avoid the unwanted dynamical phase this way.

It might also be possible to find a basis, in which the E-CD Hamiltonian can be written using only single-qubit terms. Then one could apply rotations before and after the CZ gate to transform the computational basis states in the new basis, such that the CZ gate can be applied. However, it is likely that such a basis does not exist in general or that we would need to apply entangling gates before and after, defeating the whole purpose of our gate.

Another approach we considered is taking into account higher orders of the Magnus expansion. It can be shown that terms contained in the fourth order Magnus expansion of $H_{\mathrm{E}} + H_V$ (in particular the commutator $[[[H_V, H_{\mathrm{E}}], H_{\mathrm{E}}], H_{\mathrm{E}}]$) contain the same matrix entries as the first order Magnus expansion of H_{CD}. This opens the possibility of e.g. using an approach similar to section 3.5 and imposing $M^{(1)}_{\mathrm{CD}} = M^{(2)}_{\mathrm{E}} + M^{(4)}_{\mathrm{E}}$. Usually, the fourth-order term would decay with a factor $1/\omega$ faster, than the second-order term. But since the fourth order also includes terms with H_V, we can choose V just large enough to counter the $1/\omega$. This approach might also require control of the Rydberg interaction V e.g. of the form $H_V = \cos(\omega t)V|rr\rangle\langle rr|$, which could be done by varying the distance of the Rydberg atoms using optical tweezers. However, it is difficult computing the terms of third and fourth order and we were not able to find a suitable solution yet.

One could also think about a hybrid way of using H_0 and the mean function Hamiltonian $H_{\mathrm{E,\,mean}}$. For example, one could use the $H_{\mathrm{E,\,mean}}$ as long as the mean function approximation is reasonable and switch to H_0 in between. This way one might be able to combine the benefits of both methods.

A further issue is that so far we worked with a very limited model of Rydberg atoms and assumed a closed system. Rydberg states have a finite lifetime so we need to take into account decoherence errors. An open system model with a Lindblad equation replacing the Schrödinger equation would also allow taking into account other technical sources of error like magnetic noise, errors due to finite atom temperature and laser power fluctuations. A more detailed analysis of these errors can be found in [22].

Bibliography

[1] M. Hayashi. *Quantum Information*. Springer Berlin, Heidelberg, 2006. DOI: 10.1007/3-540-30266-2.

[2] M. A. Nielsen and I. L. Chuang. *Quantum Computation and Quantum Information: 10th Anniversary Edition*. Cambridge University Press, 2010. DOI: 10.1017/CBO9780511976667.

[3] J. P. Gordon. "Quantum Effects in Communications Systems". In: *Proceedings of the IRE* 50 (1962), pp. 1898–1908. DOI: 10.1109/JRPROC.1962.288169.

[4] C. W. Helstrom. "Quantum detection and estimation theory". In: *J Stat Phys* 1 (1969), pp. 231–252. DOI: 10.1007/bf01007479.

[5] D. Deutsch. "Quantum theory, the Church–Turing principle and the universal quantum computer". In: *Proc. R. Soc. Lond. A* 400 (1985), pp. 97–117. DOI: 10.1098/rspa.1985.0070.

[6] D. Deutsch and R. Josza. "Rapid solution of problems by quantum computation". In: *Proc. R. Soc. Lond. A* 439.1907 (1992), pp. 553–558. DOI: 10.1098/rspa.1992.0167.

[7] P.W. Shor. "Algorithms for quantum computation: discrete logarithms and factoring". In: *Proceedings 35th Annual Symposium on Foundations of Computer Science*. 1994, pp. 124–134. DOI: 10.1109/SFCS.1994.365700.

[8] R. P. Feynman. "Simulating physics with computers". In: *Int J Theor Phys* 21 (1982), pp. 467–488. DOI: 10.1007/bf02650179.

[9] M. Morgado and S. Whitlock. "Quantum simulation and computing with Rydberg-interacting qubits". In: *AVS Quantum Science* 3 (2021), p. 023501. DOI: 10.1116/5.0036562.

[10] D. Ohl de Mello et al. "Defect-Free Assembly of 2D Clusters of More Than 100 Single-Atom Quantum Systems". In: *Phys. Rev. Lett.* 122 (2019), p. 203601. DOI: 10.1103/PhysRevLett.122.203601.

[11] L. Landau. "Zur Theorie der Energieubertragung". In: *Phys. Z. Sowjetunion* 2 (1932), pp. 46–51.

[12] C. Zener. "Non-adiabatic crossing of energy levels". In: *Proc. R. Soc. Lond. A* 137 (1932), pp. 696–702. DOI: 10.1098/rspa.1932.0165.

[13] E.C.G. Stueckelberg. "Theorie der unelastischen Stösse zwischen Atomen". In: *Helvetica Physica Acta* 5 (1932), pp. 369–422. DOI: 10.5169/SEALS-110177.

[14] E. Majorana. "Atomi orientati in campo magnetico variabile". In: *Nuovo Cimento* 9 (1932), pp. 43–50. DOI: doi.org/10.1007/BF02960953.

[15] T. Ehret. "Optimizing elementary quantum gates". Bachelor's Thesis. Department of Physics and Astronomy, Heidelberg University, 2022.

[16] M. Gärttner. "Many-Body Effects in Rydberg Gases : Coherent Dynamics of Strongly Interacting Two-Level Atoms and Nonlinear Optical Response of a Rydberg Gas in EIT Configuration". PhD thesis. Heidelberg University, 2014. DOI: 10.11588/HEIDOK.00015992.

[17] M. Born and V. Fock. "Beweis des Adiabatensatzes". In: *Zeitschrift für Physik* 51 (1928), pp. 165–180.

[18] V.S. Malinovsky and J.L. Krause. "General theory of population transfer by adiabatic rapid passage with intense, chirped laser pulses". In: *Eur. Phys. J. D* 14 (2001), pp. 147–155. DOI: 10.1007/s100530170212.

[19] N. V. Vitanov et al. "Stimulated Raman adiabatic passage in physics, chemistry, and beyond". In: *Rev. Mod. Phys.* 89 (2017), p. 015006. DOI: 10.1103/RevModPhys.89.015006.

[20] R. Jozsa. "Fidelity for Mixed Quantum States". In: *Journal of Modern Optics* 41 (1994), pp. 2315–2323. DOI: 10.1080/09500349414552171.

[21] D. Jaksch et al. "Fast Quantum Gates for Neutral Atoms". In: *Phys. Rev. Lett.* 85 (2000), pp. 2208–2211. DOI: 10.1103/PhysRevLett.85.2208.

[22] X. L. Zhang et al. "Fidelity of a Rydberg-blockade quantum gate from simulated quantum process tomography". In: *Phys. Rev. A* 85 (2012), p. 042310. DOI: 10.1103/PhysRevA.85.042310.

[23] M. Saffman et al. "Symmetric Rydberg controlled-Z gates with adiabatic pulses". In: *Phys. Rev. A* 101 (2020), p. 062309. DOI: 10.1103/PhysRevA.101.062309.

[24] L. S. Theis et al. "High-fidelity Rydberg-blockade entangling gate using shaped, analytic pulses". In: *Phys. Rev. A* 94 (2016), p. 032306. DOI: 10.1103/PhysRevA.94.032306.

[25] E. Urban et al. "Observation of Rydberg blockade between two atoms". In: *Nature Phys* 5 (2009), pp. 110–114. DOI: 10.1038/nphys1178.

[26] C. P. Williams. *Explorations in Quantum Computing*. Springer London, 2010. ISBN: 978-1-846-28887-6. DOI: 10.1007/978-1-84628-887-6.

[27] R. P. Feynman. "Quantum mechanical computers". In: *Found Phys* 16 (1986), pp. 507–531. DOI: 10.1007/bf01886518.

[28] D. Deutsch. "Quantum computational networks". In: *Proc. R. Soc. Lond. A* 425 (1989), pp. 73–90. DOI: 10.1098/rspa.1989.0099.

[29] T. Keating et al. "Robust quantum logic in neutral atoms via adiabatic Rydberg dressing". In: *Phys. Rev. A* 91 (2015), p. 012337. DOI: 10.1103/PhysRevA.91.012337.

[30] A. Mitra et al. "Robust Mølmer-Sørensen gate for neutral atoms using rapid adiabatic Rydberg dressing". In: *Phys. Rev. A* 101 (2020), p. 030301. DOI: 10.1103/PhysRevA.101.030301.

[31] L. F. Keary K. McDonnell and J. D. Pritchard. "Demonstration of a Quantum Gate Using Electromagnetically Induced Transparency". In: *Phys. Rev. Lett.* 129 (2022), p. 200501. DOI: 10.1103/PhysRevLett.129.200501.

[32] D. Guéry-Odelin et al. "Shortcuts to adiabaticity: Concepts, methods, and applications". In: *Rev. Mod. Phys.* 91 (2019), p. 045001. DOI: 10.1103/RevModPhys.91.045001.

[33] M. Demirplak and S. A. Rice. "Adiabatic Population Transfer with Control Fields". In: *J. Phys. Chem.* 107 (2003), pp. 9937–9945. DOI: 10.1021/jp030708a.

[34] M. V. Berry. "Transitionless quantum driving". In: *J. Phys. A: Math. Theor* 42 (2009), p. 365303. DOI: 10.1088/1751-8113/42/36/365303.

[35] M. Fleischhauer et al. "Coherent population transfer beyond the adiabatic limit: Generalized matched pulses and higher-order trapping states". In: *Phys. Rev. A* 59 (1999), pp. 3751–3760. DOI: 10.1103/PhysRevA.59.3751.

[36] F. Dou, J. Liu, and L. Fu. "High-fidelity superadiabatic population transfer of a two-level system with a linearly chirped Gaussian pulse". In: *EPL* 116 (2017), p. 60014. DOI: 10.1209/0295-5075/116/60014.

[37] F. Petiziol et al. "Fast adiabatic evolution by oscillating initial Hamiltonians". In: *Phys. Rev. A* 98 (2018), p. 043436. DOI: 10.1103/PhysRevA.98.043436.

[38] F. Petiziol et al. "Optimized three-level quantum transfers based on frequency-modulated optical excitations". In: *Sci Rep* 10 (2020). DOI: 10.1038/s41598-020-59046-8.

[39] J.R. Johansson, P.D. Nation, and F. Nori. "QuTiP 2: A Python framework for the dynamics of open quantum systems". In: *Comp. Phys. Comm.* 184 (2013), pp. 1234–1240. DOI: 10.1016/j.cpc.2012.11.019.

[40] C. R. Harris et al. "Array programming with NumPy". In: *Nature* 585 (2020), pp. 357–362. DOI: 10.1038/s41586-020-2649-2.

[41] F. Petiziol and S. Wimberger. "Effect of Phase Errors on a Quantum Control Protocol Using Fast Oscillations". In: *Condens. Matter* 4 (2019), p. 34. DOI: 10.3390/condmat4010034.

[42] C.J. Foot. *Atomic Physics*. Oxford univeristy press, 2004. ISBN: 9780198506966. URL: https://global.oup.com/ukhe/product/atomic-physics-9780198506966.

[43] M. Mohseni, A. T. Rezakhani, and D. A. Lidar. "Quantum-process tomography: Resource analysis of different strategies". In: *Phys. Rev. A* 77 (2008), p. 032322. DOI: 10.1103/PhysRevA.77.032322.

[44] J.R. Johansson et al. *QuTiP: Quantum Toolbox in Python*. 2022. URL: https://qutip.org/documentation.html.

A Appendix

A.1 Dependency on the ECD frequency

How well E-CD driving performs depends heavily on the E-CD frequency ω. It was previously mentioned that higher-order Magnus terms contribute with higher orders in $1/\omega$. The next terms we neglect are of order $1/\omega^2$ so it is expected that the diabatic errors should decrease proportionally to $1/\omega^2$. This can also be checked by plotting the fidelity as a function of the E-CD frequency as in Fig. A.1 for the E-CD-driven Landau-Zener protocol. We produced similar results for an E-CD-driven STIRAP protocol.

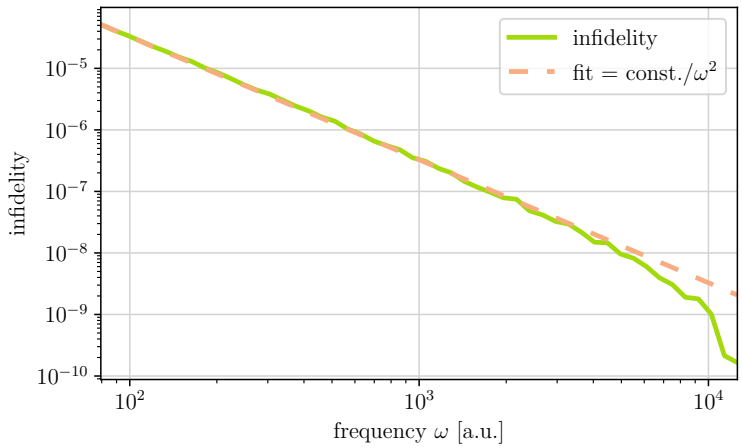

Figure A.1: Infidelity of the E-CD-driven Landau-Zener system with ARP pulses as a function of the ECD frequency ω. The irregular behavior for large ω is presumably because we reach the numerical limit of the simulation. The Gaussian pulse is normalized to 5 and the detuning is linear with $\Delta_{\max} = 20$ MHz.

A.2 CD Hamiltonian for $V \to \infty$

In this section, we derive the eigenvectors of the 3×3 matrix from section 3.1. In (3.4) the 3×3 matrix was rewritten as

$$\begin{pmatrix} 0 & \sqrt{2}\Omega & 0 \\ \sqrt{2} & 2\Delta & \sqrt{2}\Omega \\ 0 & \sqrt{2}\Omega & 4\Delta+2V \end{pmatrix} = V\left[\underbrace{\begin{pmatrix} 0 & & \\ & 0 & \\ & & 2 \end{pmatrix}}_{:=H_0} + \frac{1}{V}\underbrace{\begin{pmatrix} 0 & \sqrt{2}\Omega & 0 \\ \sqrt{2} & 2\Delta & \sqrt{2}\Omega \\ 0 & \sqrt{2}\Omega & 4\Delta \end{pmatrix}}_{:=H_1}\right] \tag{A.1}$$

$$=: V\left(H_0+\varepsilon H_1\right) \tag{A.2}$$

Where we defined $\varepsilon := 1/V$. The eigenvector equation then reads

$$\left(H_0+\varepsilon H_1\right)v = \lambda v. \tag{A.3}$$

Inserting the pertubational approach $v = v_0+\varepsilon v_1$ and $\lambda = \lambda_0+\varepsilon\lambda_1$ allows us to write down the eigenequations in first order of ε

$$H_0 v_0 = \lambda_0 v_0 \tag{A.4}$$

$$H_0 v_1 + H_1 v_0 = \lambda_0 v_1 + \lambda_1 v_0. \tag{A.5}$$

Since H_0 has two obvious eigenvalues $\lambda_0 = 0$ and $\lambda_0 = 2$ we can make a case distinction.

(i) In the case $\lambda_0 = 0$ from equation (A.4) follows directly that $v_0^{(3)} = 0$. Equation (A.5) becomes

$$\begin{pmatrix} 0 \\ 0 \\ 2v_1^{(3)} \end{pmatrix} + \begin{pmatrix} 0 & \sqrt{2}\Omega & 0 \\ \sqrt{2}\Omega & 2\Delta & \sqrt{2}\Omega \\ 0 & \sqrt{2}\Omega & 4\Delta \end{pmatrix}\begin{pmatrix} v_0^{(1)} \\ v_0^{(2)} \\ 0 \end{pmatrix} = \lambda_1 \begin{pmatrix} v_0^{(1)} \\ v_0^{(2)} \\ 0 \end{pmatrix} \tag{A.6}$$

We can always fulfill the third line by choosing $v_1^{(3)} = -\frac{\Omega}{\sqrt{2}}v_0^{(2)}$. The first two lines reduce to a 2×2 matrix problem, which is essentially the Landau-Zener problem with $\Omega \to \sqrt{2}\Omega$. The solution to this can therefore be taken from (2.29), with a slightly different angle of

$$\theta' = \frac{1}{2}\arctan\left(-\sqrt{2}\frac{\Omega}{\Delta}\right). \tag{A.7}$$

Thus, the two possible solutions read

$$\{v\} = \left\{ \begin{pmatrix} -\sin(\theta') \\ \cos(\theta') \\ -\frac{\Omega}{\sqrt{2}V}\cos(\theta') \end{pmatrix}, \begin{pmatrix} \cos(\theta') \\ \sin(\theta') \\ -\frac{\Omega}{\sqrt{2}V}\sin(\theta') \end{pmatrix} \right\} \tag{A.8}$$

(i) In the second case $\lambda_0 = 2$, equation (A.4) turns into

$$\begin{pmatrix} 0 \\ 0 \\ 2v_0^{(3)} \end{pmatrix} = 2 \begin{pmatrix} v_0^{(1)} \\ v_0^{(2)} \\ v_0^{(3)} \end{pmatrix}, \tag{A.9}$$

such that $v_0^{(1)} = v_0^{(2)} = 0$. The second eigenvalue equation then turns into

$$\begin{pmatrix} 0 \\ 0 \\ 2v_1^{(3)} \end{pmatrix} + \begin{pmatrix} 0 & \sqrt{2}\Omega & 0 \\ \sqrt{2}\Omega & 2\Delta & \sqrt{2}\Omega \\ 0 & \sqrt{2}\Omega & 4\Delta \end{pmatrix} \begin{pmatrix} v_0^{(1)} \\ v_0^{(2)} \\ 0 \end{pmatrix} = \lambda_1 \begin{pmatrix} 0 \\ 0 \\ v_0^{(3)} \end{pmatrix} + 2 \begin{pmatrix} v_1^{(1)} \\ v_1^{(2)} \\ v_1^{(3)} \end{pmatrix}. \tag{A.10}$$

The first line gives $v_1^{(1)} = 0$ and the second line $\sqrt{2}\Omega v_0^{(3)} = 2v_1^{(2)}$. The third line only gives a value for λ_1, but does not impose any restrictions on $v_1^{(3)}$. We may just chose $v_1^{(3)} = 0$ since it is negligible as $v_0^{(3)} \neq 0$. The solution to the eigenvalue problem is then

$$v = v_0^{(3)} \begin{pmatrix} 0 \\ \frac{\Omega}{\sqrt{2}V} \\ 1 \end{pmatrix}. \tag{A.11}$$

Introducing $\nu := \frac{\Omega}{\sqrt{2}V}$, the up to $1/V$ normalized eigenvectors are

$$\{v\} = \left\{ \begin{pmatrix} -\sin\theta' \\ \cos\theta' \\ -\nu\cos\theta' \end{pmatrix}, \begin{pmatrix} \cos\theta' \\ \sin\theta' \\ -\nu\sin\theta' \end{pmatrix}, \begin{pmatrix} 0 \\ \nu \\ 1 \end{pmatrix} \right\}. \tag{A.12}$$

A.3 Second order Magnus expansion

General case

Before looking at specific systems, we aim to calculate the second-order Magnus expansion for a general E-CD Hamiltonian of the form in (2.36) (remember that here T is not the protocol time):

$$\begin{aligned}
M_{\mathrm{E}}^{(2)}(T) &= -\frac{1}{2}\left(\frac{i}{\hbar}\right)^2 \int_{t_n}^{t_n+T} \mathrm{d}t' \int_{t_n}^{t'} \mathrm{d}t'' \, [H_{\mathrm{E}}(t'), H_{\mathrm{E}}(t'')] \\
&= -\frac{\omega}{2} \int_{t_n}^{t_n+T} \mathrm{d}t' \int_{t_n}^{t'} \mathrm{d}t'' \sum_{i,j} c_i(t') c_j(t'') \underbrace{[H_i, H_j]}_{=:i\rho_{ij}} \\
&= -i\frac{\omega}{2} \sum_{i\neq j} \int_0^T \mathrm{d}t' \int_0^{t'} \mathrm{d}t'' \sum_{k,l=1}^{L} \left(A_{ik}(t_n)\sin(k\omega t') + B_{ik}(t_n)\cos(k\omega t')\right) \\
&\quad \times \left(A_{jl}(t_n)\sin(l\omega t'') + B_{jl}(t_n)\cos(l\omega t'')\right) \rho_{ij} \\
&= -i\frac{\omega}{2} \sum_{i\neq j} \sum_{k,l=1}^{L} \int_0^T \mathrm{d}t' \, \frac{1}{k\omega} \left(A_{ik}(t_n)\sin(k\omega t') + B_{ik}(t_n)\cos(k\omega t')\right) \\
&\quad \times \left(-A_{jl}(t_n)\cos(l\omega t') + B_{jl}(t_n)\sin(l\omega t') + A_{jl}(t_n)\right) \rho_{ij}.
\end{aligned} \tag{A.13}$$

In the third step we assumed the coefficients A_{ik} and B_{ik} to be approximately constant in the interval $[t_n, t_n + T]$, which is reasonable in the limit of large ω. In the following we will drop the argument of these coefficients for the sake of shorter notation. Next we can make use of the fact that $\sin(kx)$ and $\cos(kx)$ are orthonormal with the integral from 0 to 2π as the inner product. Therefore, the only nonzero terms are the ones involving $\sin^2(k\omega t')$ and $\cos^2(k\omega t')$

$$\begin{aligned}
M_{\mathrm{E}}^{(2)}(T) &= -i\frac{1}{2} \sum_{i\neq j} \sum_{k=1}^{L} \frac{1}{k} \int_0^T \mathrm{d}t' \, \left(A_{ik}B_{jk}\sin^2(k\omega t') - B_{ik}A_{jk}\cos^2(k\omega t')\right) \rho_{ij} \\
&= -i\frac{1}{2} \sum_{i\neq j} \sum_{k=1}^{L} \frac{1}{k}\frac{\pi}{\omega} \left(A_{ik}B_{jk} - B_{ik}A_{jk}\right) \rho_{ij} \\
&= -i\frac{T}{4} \sum_{k=1}^{L} \frac{1}{k} \left[\sum_{i<j} \left(A_{ik}B_{jk} - B_{ik}A_{jk}\right) \rho_{ij} + \sum_{i>j} \left(A_{ik}B_{jk} - B_{ik}A_{jk}\right) \rho_{ij}\right] \\
&= -i\frac{T}{4} \sum_{k=1}^{L} \frac{1}{k} \sum_{i<j} \left[\left(A_{ik}B_{jk} - B_{ik}A_{jk}\right) \rho_{ij} + \left(A_{jk}B_{ik} - B_{jk}A_{ik}\right) \rho_{ji}\right].
\end{aligned} \tag{A.14}$$

Using the commutator property $\rho_{ij} = -\rho_{ji}$, the final result is

$$M_{\mathrm{E}}^{(2)}(T) = -i\frac{T}{2}\sum_{i<j}\sum_{k=1}^{L}\frac{1}{k}\left(A_{ik}B_{jk} - B_{ik}A_{jk}\right)\rho_{ij}. \tag{A.15}$$

ECD for the Landau Zener System

We now want to determine $M_{\mathrm{E}}^{(2)}(T)$ in the case of the Landau-Zener System with the ansatz (2.37):

$$H_{\mathrm{E}}(t) = c_1(t)\sigma_z + c_2(t)\sigma_x. \tag{A.16}$$

The second order Magnus expansion can be obtained using formula (A.15) for which we need the commutators ρ_{ij}. In this simple case we only have one namely

$$i\rho_{12} = [\sigma_z, \sigma_x] = i\sigma_y. \tag{A.17}$$

Fixing $L = 1$ we obtain

$$M_{\mathrm{E}}^{(2)}(T) = -i\frac{T}{2}(A_{11}B_{21} - B_{11}A_{21})\sigma_y. \tag{A.18}$$

E-CD for the adiabatic CZ gate

For the E-CD driving of the adiabatic CZ gate we made the ansatz (3.13) which we will here simply write as $H_E(t) = \sqrt{\omega}(c_1(t)H_1 + c_2(t)H_2 + c_3(t)H_3)$. Without going into detail, one finds that

$$\begin{aligned} i\rho_{12} &= [H_1, H_2] = 0, \\ i\rho_{13} &= [H_1, H_3] = i(\sigma_y \otimes P_0 + P_0 \otimes \sigma_y), \\ i\rho_{23} &= [H_2, H_3] = i(\sigma_y \otimes P_1 + P_1 \otimes \sigma_y). \end{aligned} \tag{A.19}$$

In our case it suffices to fix $L = 1$, such that by applying (A.15) the second order Magnus term reduces to

$$M_{\mathrm{E}}^{(2)}(T) = -i\frac{T}{2}\left[\left(A_{11}B_{31} - B_{11}A_{31}\right)\rho_{13} + \left(A_{21}B_{31} - B_{21}A_{31}\right)\rho_{23}\right]. \tag{A.20}$$

Realizing that the commutators are the matrices that make up the CD Hamiltonian, we can write $H_{\mathrm{CD}}(t) = f_1(t)\rho_{13} + f_2(t)\rho_{23}$. The left-hand side of the equation is then easily determined

$$\begin{aligned} M_{\mathrm{CD}}^{(1)}(T) &= -i\int_{t_n}^{t_n+T} \mathrm{d}t'\; H_{\mathrm{CD}}(t') = -i\int_{t_n}^{t_n+T} \mathrm{d}t'\; f_1(t')\rho_{13} + f_2(t')\rho_{23} \\ &= -iT\left(f_1(t_n)\rho_{13} + f_2(t_n)\rho_{23}\right) \end{aligned} \tag{A.21}$$

where in the last line we assumed f_1 and f_2 to be approximately constant on the timescale T. One can read off the set of equations as already presented in (3.15):

$$A_{11}B_{31} - B_{11}A_{31} = 2f_1, \qquad A_{21}B_{31} - B_{21}A_{31} = 2f_2. \tag{A.22}$$

A.4 Fidelity improvement by E-CD driving for equal pulses

In section 3.2 we found that the usage of an E-CD Hamiltonian for the adiabatic CZ gate provides significant fidelity improvements compared to the original protocol. We also remarked that the E-CD Hamiltonian tends to use larger pulses, such that it would be fairer to compare the fidelities with the E-CD frequency ω limited so that $H_E \sim H_0$.
In particular, the amplitudes of the entires in H_E are $\sqrt{2\omega|f_1(t)|}$ and $\sqrt{2\omega|f_1(t)|}$. The highest pulse amplitude used for the E-CD driving is thus $\Omega_{\mathrm{E,\,max}} = \max_{t,i}\{\sqrt{2\omega|f_i(t)|}\}$, a condition for equal pulse heights would then be $\Omega_{\max} = \Omega_{\mathrm{E,\,max}}$. After defining $f_{\max} := \max_{t,i}\{f_i(t)\}$, we can meet the condition by choosing

$$\omega = \frac{\Omega_{\max}^2}{2f_{\max}}. \tag{A.23}$$

The results of this can be seen in Fig. A.2. Fixing the pulse height restricts the power of E-CD driving and limits the regions in which it provides an advantage over the original protocol. For limited Rydberg blockades and large pulses, the unwanted phase error appears to be the

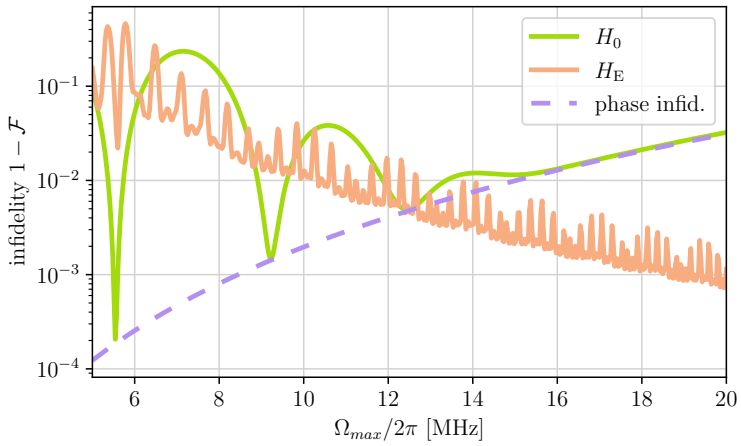

Figure A.2: Infidelity of the CZ gate with initial state $(|00\rangle + |11\rangle)/\sqrt{2}$ using the protocol as proposed by Saffman et al. (green) compared to using the ECD CZ protocol (orange). We also plotted the infidelity we would expect purely from the unwanted dynamical phase (purple). The parameters are $T = 0.54\ \mu$s and $\Delta_{\max}/\Omega_{\max} = 23/17$ as in the Saffman paper and $V = 1200$ MHz.

largest issue so that fidelity can be improved significantly by using the suggested E-CD gate. In domains where the unwanted phase is not the leading issue, the original protocol produces peaks to much lower infidelities, while on average both methods appear to produce similar fidelities.

Erklärung

Ich versichere, dass ich diese Arbeit selbstständig verfasst und keine anderen als die angegebenen Quellen und Hilfsmittel benutzt habe.

Heidelberg, den 24.03.2023,